The Hot and Cold Properties of Nuclear Matter

Khaled Hassaneen[1,2,*]**, Hesham Mansour**[3]

[1]Department of Physics, Faculty of Science, Sohag University, Sohag, Egypt
[2]Department of Physics, Faculty of Science, Taif University, Taif, Saudi Arabia
[3]Department of Physics, Faculty of Science, Cairo University, Gizza, Egypt

Abstract   The properties of nuclear matter at zero and finite temperatures in the frame of the Brueckner theory realistic nucleon-nucleon potentials are studied. Comparison with other calculations is made. In addition we present results for the symmetry energy obtained with different potentials, which is of great importance in astrophysical calculation. Properties of asymmetric nuclear matter are derived from various many-body approaches. This includes phenomenological ones like the Skyrme Hartree-Fock and relativistic mean field approaches, which are adjusted to fit properties of nuclei, as well as more microscopic attempts like the BHF approximation, a Self-Consistent Greens Function (SCGF) method and the so-called V_{lowk} approach, which are based on realistic nucleon-nucleon interactions which reproduce the nucleon-nucleon phase shifts. These microscopic approaches are supplemented by a density-dependent contact interaction to achieve the empirical saturation property of symmetric nuclear matter. Special attention is paid to behavior of the isovector and the isoscalar component of the effective mass in neutron-rich matter. The nuclear symmetry potential at fixed nuclear density is also calculated and its value decreases with increasing the nucleon energy. In particular, the nuclear symmetry potential at saturation density changes from positive to negative values at nucleon kinetic energy of about 200 MeV. The hot properties of nuclear matter are also calculated using T^2–approximation method at low temperatures. Good agreement is obtained in comparison with previous theoretical estimates and experimental data especially at low densities.

Keywords   Brueckner-Hartree-Fock Approximation, Self-Consistent Greens Function (SCGF) Method, Three-body Forces, Symmetry Energy, Symmetry Potential, Effective Mass, T^2–approximation Method

1. Introduction

One of the most fundamental problems in nuclear many-body theory is the attempt to evaluate the nuclear matter binding energy and saturation properties, starting from a realistic Nucleon-Nucleon (NN) interaction with no free parameters. In fact a lot of work has been done trying to solve this problem using different approaches and methods which are discussed in details by Müther and Polls[1]. An important ingredient of all these approaches is the consideration of the two-nucleon correlations which are induced by the strong short-range components of the NN interaction. In lowest-order Brueckner theory, the familiar Brueckner-Hartree-Fock (BHF) approach, is adopted to calculate the energy, the so-called G-matrix for evaluating the energy in the Hartree-Fock approach. In the G-matrix one accounts for the particle-particle correlations which means the scattering of two nucleons from states which are occupied in the Slatter determinant describing the ground state, into unoccupied particle states above the Fermi surface[2-4].

The potentials we will employ here are the recent models of the Nijmegen group[5], the Argonne V18 potential[6] and the charge-dependent Bonn potential (CD-Bonn)[7]. The recent versions of The Nijmegen group are Nijm-I, Nijm-II and Reid93 potentials. Although all these potentials predict almost identical phase shifts, their mathematical structure is quite different.

Most of the microscopic calculations have been addressed to study symmetric matter[2] and pure neutron matter[8,9]. The study of asymmetric nuclear matter is technically more involved and only few Brueckner-Hartree-Fock (BHF) calculations are available[4,10,11]. The BHF approximation includes the self-consistent procedure of determining the single-particle auxiliary potential, as first devised by Brueckner and Gammel[12], which is an essential ingredient of the method. Different approaches have been used to study the EoS of asymmetric nuclear matter including Dirac-Brueckner-Hartree-Fock (DBHF) calculations[13-16], Brueckner-Hartree-Fock (BHF) approximation to Brueckner-Bethe-Goldstone (BBG) calculations[17,18] and variational methods[19,20]. Besides these microscopic approaches, effective theories such as Relativistic Mean Field (RMF) theory[21,22] and non-relativistic effective interactions[23,24] have also been used extensively to study the EoS and mean field properties of the asymmetric nuclear matter.

As it is well known, the BHF approximation largely violates the Hugenholtz-Van Hove (HVH) theorem[26], which basically measures the consistency of a given order of approximation in a perturbative approach. In symmetric nuclear matter, the inclusion of the so-called hole-hole (hh) contribution greatly improves the fulfillment of the HVH theorem[27]. We use realistic NN forces and operate within SCGF framework. It is well known that the selfconsistent BHF approach does not reproduce the correct saturation point of nuclear matter with only the inclusion of the two-body interaction[28,29]. But our attention is mainly focused on how nuclear matter properties change in terms of the asymmetry ratio and some caution has to be taken whenever saturation properties are involved. In addition, it gives a simple microscopic justification of the empirical laws governing asymmetric nuclear matter.

1.1. In the Present Report

In order to establish the importance of the hh term in the calculation of EoS for asymmetric nuclear matter our aim is to extend the BHF approach which ignores the hh term to SCGF approach, which includes the hh term. It has been shown, in the case of pure neutron matter[30] and also symmetric nuclear matter[2,30] that the new terms give a large contribution to single-particle properties like the mean field and the nucleon effective mass. We will refer to the present approach to compute nuclear single-particle properties as SCGF approximation[2,4].

The nuclear matter symmetry energy, which is defined as the difference in energy per nucleon between the pure neutron matter and the symmetric nuclear matter, is an important quantity that determines the properties of objects such as the atomic nucleus and the neutron star[31]. The study of symmetry energy and its dependence on nuclear density and temperature is currently a subject of great interest[32]. Theoretically, the symmetry energy can be determined from microscopic calculations such as the Self-Consistent Green Function (SCGF) and the Dirac-Brueckner-Hartree-Fock (DBHF) calculations, or the phenomenological calculations such as the Skyrme Hartree-Fock (SHF) and the Relativistic Mean Field (RMF) calculations[4, 31, 33-35]. These calculations currently predict wide range of symmetry energies for densities below and above normal nuclear density, $\rho_0 = 0.16 \text{fm}^{-3}$. Also, the symmetry energy and its relation with the chemical potential have been studied.

Also, the properties of asymmetric nuclear matter are derived from various many-body approaches. This includes phenomenological ones like the Skyrme Hartree-Fock and relativistic mean field approaches, which are adjusted to fit properties of nuclei, as well as more microscopic attempts like the Brueckner-Hartree-Fock approximation, a self-consistent Greens function method and the so-called V_{lowk} approach. These microscopic approaches are supplemented by a density-dependent contact interaction to achieve the empirical saturation property of symmetric

nuclear matter. The predictions of the isovector component of the effective mass in neutron-rich matter, the symmetry potential and symmetry energy are discussed.

The one-body potentials for protons and neutrons are obtained from the self-consistent Green-function calculations of asymmetric nuclear matter, in particular their dependence on the degree of proton/neutron asymmetry. Results of the binding energy per nucleon as a function of the density and asymmetry parameter are presented for the self-consistent Green function approach using the CD-Bonn potential. The nuclear symmetry potential at fixed nuclear density is also calculated and its value decreases with increasing the nucleon energy. The isoscalar proton/neutron effective mass splitting in neutron-rich matter has been studied.

Recently, Li *et al.*[36] have studied the saturation properties of nuclear matter within the Brueckner-Hartree-Fock approach using continuous single particle energies and employing the most recent accurate nucleon-nucleon potentials. They found that their results confirm the concept of "Coester line" or "Coester band", i.e., density and energy of the various saturation points being strongly correlated, yielding either a too large saturation density or a too small binding energy.

The many-body method we will employ in deriving the EoS of both symmetric and pure nuclear matter is a rather simple one i.e., the non-relativistic BHF method with a conventional and continuous single particle spectrum using different modern NN potentials.

The results in the present work which come out by approximating the single particle self-consistent potential with a parabolic form.

1.2. The Theoretical Model

1.2.1. Brueckner-Hartree-Fock for Symmetric Nuclear Matter

In the BHF approximation, the nuclear matter total energy E_A is obtained from the Brueckner G-matrix, $G(\omega)$, according to the equation:

$$E_A = \sum_{k_1 < k_F} \frac{\hbar^2 k_1^2}{2m} + \frac{1}{2} \sum_{k_1, k_2 < k_F} \left\langle k_1 k_2 \mid G\left(e_{k_1} + e_{k_2}\right) \mid k_3 k_4 \right\rangle a \quad (1)$$

with $|k_1 k_2\rangle_a = |k2k1\rangle$, i.e., the subscript a indicates antisymmetrization of the matrix elements. Here k_F is the Fermi momentum, the summation over the momenta k_i include spin and isospin variables. The single particle energies e_k, appearing in the entry energy of the G-matrix, are given by:

$$e(k) = \frac{\hbar^2 k^2}{2m} + U(k) \quad (2)$$

Where, the single particle potential $U(k)$ is determined by the self-consistent equation:

$$U(k) = \sum_{k' < k_F} \left\langle kk' \mid G\left(e_{k_1} + e_{k_2}\right) \mid kk' \right\rangle \quad (3)$$

The self-consistency is coupled with the integral equation for the G-matrix, i.e., in the BHF approach $G(\omega)$ is obtained by solving the Bethe-Goldstone equation:

$$\langle k_1 k_2 | G(\omega) | k_3 k_4 \rangle = \langle k_1 k_2 | \upsilon | k_3 k_4 \rangle +$$

$$\sum_{k_3' k_4'} \langle k_1 k_2 | \upsilon | k_3' k_4' \rangle \frac{\left(1 - \Theta_F(k_3')\right)\left(1 - \Theta_F(k_4')\right)}{\omega - e_{k_3'} - e_{k_3'}} \quad (4)$$

$$\langle k_3' k_4' | G(\omega) | k_3 k_4 \rangle$$

where, $\Theta_F(k) = 1$ defining the step function for $k < k_F$ and is zero otherwise and ω denotes the starting energy. The product $Q(k, k') = (1 - \Theta_F(k))(1 - \Theta_F(k'))$, appearing in the kernel of Equation (4), enforces the scattered momenta to lie outside the Fermi sphere and it is commonly referred to as the "Pauli operator". In the case of the angle-average of Pauli operator this energy is given as,[37]

$$E_A = \frac{3k_F^2}{52m} + \frac{6}{k_F^3} \sum_{T,S,I,J} (2T+1)(2J+1) \int_0^{k_F} dk\, k^2$$

$$\left[\int_0^{k_F - k} dK\, K^2 + \int_{k_F - k}^{\sqrt{k_F^2 - k^2}} dK\, K^2 \frac{k_F^2 - K^2 - k^2}{2Kk} \right] \quad (5)$$

$$\langle klJ | G_{ST}(\omega, K) | KlJ \rangle$$

If one assumes that the potential $U(k)$, or equivalently the single particle energy $e(k)$, has approximately a quadratic form

$$e(k) \approx e_0 + \frac{\hbar^2 k^2}{2m^*} \quad (6)$$

where, e_0 is the zero point energy. Then one can calculate the potential, at each iteration step, in few points only and interpolate the obtained values with a parabola. The approximation of Eq. (6) is usually called the effective mass approximation, since then the spectrum has the same shape as the free one but with an effective mass m^*. From Equations (2) and (6) the effective mass m^* can be evaluated from the slope of $U(k)$ at the Fermi momentum[38],

$$\frac{m^*}{m} = \left[1 + \frac{m}{\hbar^2 k} \frac{dU}{dk} \right]_{k=k_F}^{-1} \quad (7)$$

1.3. Brueckner-Hartree-Fock for Asymmetric Nuclear Matter

The self-energy of a nucleon with isospin i, momentum k and energy ω in asymmetric nuclear matter is defined in the BHF approximation by[1, 4],

$$\sum_i^{BHF} = \sum_j \int d^3 q \langle kq | G(\Omega) | kq \rangle_{ij}\, n_j^0(q). \quad (8)$$

In this equation $n_j^0(q)$ refers to the occupation probability of a free Fermi gas of protons (j = p) and neutrons (j = n) like in the mean-field or Hartree-Fock approach. This means that for asymmetric matter with a total density $\rho = \rho_p + \rho_n$ this probability is defined by:

$$n_j^0(q) = \begin{cases} 1 & \text{for } |q| \le k_{Fj}, \\ 0 & \text{for } |q| > k_{Fj}, \end{cases} \quad (9)$$

With Fermi momenta for protons (k_{Fp}) and neutrons (k_{Fn}).

The antisymmetrized G matrix elements in Eq. (8) are obtained from a given NN interaction by solving the Bethe-Goldstone equation:

$$\langle kq | G(\Omega) | kq \rangle_{ij} = \langle kq | V | kq \rangle_{ij}$$

$$+ \int d^3 p_1 d^3 p_2 \langle kq | V | p_1 p_2 \rangle_{ij}$$

$$\times \frac{Q(p_1 i, p_2 j)}{\Omega - \left(\varepsilon_{p1,i} + \varepsilon_{p2,j} \right) + i\eta} \times \langle p_1 p_2 | G(\Omega) | kq \rangle_{ij} \quad (10)$$

The single-particle energies ε_{pi} of the intermediate states should be the corresponding BHF single-particle energies which are defined in terms of the real part of the BHF self-energy of Eq. (8) by:

$$\varepsilon_{ki} = \frac{k^2}{2m} + \text{Re}\left[\sum_i^{BHF}\left(k, \omega = \varepsilon_{ki}\right) \right] \quad (11)$$

with a starting energy parameter $\Omega = \omega + \varepsilon_{qj}$ in the Bethe-Goldstone Eq. (10).

1.4. Self-Consistent Green's Function

One of the drawbacks of the BHF approximation is the fact that it does not provide results for the equation of state, which are consistent from the point of view of thermodynamics. As an example we mention that BHF results do not fulfill e.g., the Hugenholtz van Hove theorem. This is due to the fact that the BHF approximation does not consider the propagation of particle and hole states on equal footing. An extension of the BHF approximation, which obeys this symmetry is the Self-Consistent Green's Function (SCGF) method. During the last years techniques have been developed, which allow to evaluate the solution of the SCGF equations for microscopic NN interactions. Those calculation demonstrate that for the case of realistic NN interactions, the contribution of particle-particle ladders dominates the contribution of corresponding hole-hole propagation terms. This justifies the use of the BHF approximation and a procedure, which goes beyond BHF and accounts for hole-hole terms in a perturbative way[2, 39]. This leads to a modification of the self-energy in the BHF approximation by adding a hole-hole term of the form:

$$\Delta \sum_i^{2h1p}(k, \omega) = \sum_j \int_{k_{Fj}}^{\infty} d^3 p \int_0^{k_{Fi}} d^3 h_1 \int_0^{k_{Fj}} d^3 h_2$$

$$\times \frac{\langle kp | G(\Omega) | h_1 h_2 \rangle_{ij}^2}{\omega + \varepsilon_{pj} - \varepsilon_{h1i} - \varepsilon_{h2j} - i\eta} \quad (12)$$

The quasi-particle energy for the extended self-energy can be defined as:

$$\varepsilon_{ki}^{qp} = \frac{k^2}{2m} + Re\left[\sum_i^{BHF}\left(k, w = \varepsilon_{ki}^{qp}\right) + \Delta\sum_\tau^{2h1p}\left(k, \omega = \varepsilon_{ki}^{qp}\right)\right], \quad (13)$$

Accordingly, the Fermi energy is obtained evaluating this definition at the Fermi momentum k = k_{Fi} for protons and neutrons, respectively:

$$\varepsilon_{Fi} = \varepsilon_{kFi}^{qp} \quad (14)$$

The spectral functions for hole and particle strength, $S_i^h(k,w)$ and $S_i^p(k,w)$, are obtained from the real and imaginary part of the self-energy $\sum = \sum^{BHF} + \Delta\sum^{2h1p}$:

$$S_i^{h(p)}(k,\omega) = \pm\frac{1}{\pi}\frac{Im\sum_i(k,\omega)}{\left[\omega - k^2/2m - Re\sum_i(k,\omega)\right]^2 + \left[Im\sum_i(k,\omega)\right]^2} \quad (15)$$

where, the plus and minus sign on the left-hand side of this equation refers to the case of hole (h, $\omega<\varepsilon_{Fi}$) and particle states (p, $\omega>\varepsilon_{Fi}$), respectively. The hole strength represents the probability that a nucleon with isospin i, momentum k and energy ω can be removed from the ground state of the nuclear system with the removal energy ω, whereas the particle strength denotes the probability that such a nucleon can be added to the ground state of the system with A nucleons resulting in a state of the A+1 particle system which has an energy of ω relative to the ground state of the A particle system. Hence the occupation probability is obtained by integrating the hole part of the spectral function:

$$n_i(k) = \iint_{-\infty}^{\varepsilon_{Fi}} d\omega S_i^h(k,\omega). \quad (16)$$

Note that this yields values for the occupation probability, which ranges between values of 0 and 1 for all momenta k, leading to a partial depletion of the hole-states in the Fermi gas model (k<k_F) and partial occupations for states with momenta h>k_F. A similar integral yields the mean energy for the distribution of the hole and particle strength, respectively:

$$\left\langle\varepsilon_{hi}(k)\right\rangle = \frac{\int_{-\infty}^{\varepsilon_{Fi}} d\omega\,\omega S_i^h(k,\omega)}{n_i(k)} \quad (17)$$

$$\left\langle\varepsilon_{pi}(k)\right\rangle = \frac{\int_{\varepsilon_{Fi}}^{\infty} d\omega\,\omega S_i^p(k,\omega)}{1 - n_i(k)} \quad (18)$$

Our self-consistent Green's function calculation is defined by identifying the single particle energy in the Bethe-Goldstone equation as well as in the 2h1p correction term in Eq. (12):

$$\varepsilon_{k\tau} = \begin{cases} \varepsilon_{h\tau}(k\rangle) & \text{for } k < k_{F\tau} \\ \varepsilon_{p\tau}(k\rangle) & \text{for } k > k_{F\tau} \end{cases} \quad (19)$$

This definition leads to a single particle Greens function, which is defined for each momentum k by just one pole at $\omega = \varepsilon_{k\tau}$. Hence, the total energy per nucleon is evaluated by:

$$\frac{E}{A} = \frac{\sum_i \int d^3k \int_{-\infty}^{\varepsilon_{Fi}} d\omega S_i^h(k,\omega)(k,\omega)(k^2/2m + \omega)/2}{\sum_i \int d^3k n_i(k)} \quad (20)$$

In order to achieve saturation in nuclear matter one has to add three-body interaction terms or a density-dependent two-nucleon interaction. So, it is quite natural to supplement the effective interaction by a simple contact interaction, which we have chosen following the notation of the Skyrme interaction to be of the form:

$$\Delta H = \frac{1}{2}t_0\,\rho^2 + \frac{1}{12}t_3\rho^{2+\delta}, \quad (21)$$

where, ρ is the matter density, t_0, t_3 and δ are parameters. For a fixed value of δ (typically $\delta = 0.5$) we have fitted t_0 and t_3 in such a way that a Hartree-Fock calculation using V_{lowk} plus the contact term of Eq. (21) yields the empirical saturation point for symmetric nuclear matter.

The same parameterization of a contact term has been used to evaluate corrections to the self-energy of BHF and SCGF in such a way that also these calculations reproduce the saturation of symmetric nuclear matter.

The many–body problem at finite temperatures has been considered by several authors within different approaches, such as the finite temperature Green's function method[40], the thermo field method[41], or the Bloch–De Domicis (BD) diagrammatic expansion[42]. The latter, was developed soon after the Brueckner theory, represents the "natural" extension to finite temperature of the BBG expansion, to which it leads in the zero temperature limit. Baldo and Ferreira[43] showed that the dominant terms in the BD expansion were those that correspond to the zero temperature of the Brueckner–Bethe–Goldstone (BBG) diagrams, where the temperature is introduced only through the Fermi–Dirac distribution

$$f(k,T) = \left[1 + exp\left(\frac{e(k,T) - \mu(T)}{T}\right)\right]^{-1}. \quad (22)$$

Therefore, at the BHF level, finite temperature effects can be introduced in a very good approximation just replacing in the BGE (4):

(i) the zero temperature Pauli operator $Q=(1-\theta_1(k))(1-\theta_2(k))$ by the corresponding finite temperature one $Q(T)=(1-f_1)(1-f_2)$,

(ii) The single–particle energies $e(k)$ by the temperature dependent ones $e(k, T)$), obtained from Eqs. (3) and (4) when $\theta(k)$ is replaced by $f(k, T)$.

In the present work, two simplifications are used to calculate the thermodynamic properties of nuclear matter.

Firstly, the G-matrix calculation is performed at $T = 0$ MeV and using the continuous choice for $U(k)$. Secondly, the internal energy of the system $F \rightarrow F/A$, is computing by using the entropy of the free Fermi gas with effective mass m^*, where the internal energy of nuclear mater is defined by

$$F = E - TS_T, \qquad (23)$$

where $E \rightarrow E/A$ is the total energy at $T = 0$, S_T is the entropy of the system at temperature T. In addition thermal effects are treated in a low temperature limit of the internal energy. Starting from Eq. (23), in the low temperature limit the energy and entropy behave as $E = E_{T=0} + aT^2$ and $S_T = 2aT$, respectively, where a is the so–called level density parameter. Therefore, for the internal energy we have the following expression:

$$F = E + aT^2 - 2aT^2 = E - a(\rho)T^2 \qquad (24)$$

with

$$a(\rho) = \frac{1}{4}\pi^2 \left(\frac{2m^*(k_F)}{\hbar^2 k_F^2} \right)$$

$$= \frac{1}{6}\left(\frac{2m^*(\rho)}{\hbar^2} \right)\left(\frac{3\pi^2}{2} \right)^{1/3} \rho^{-2/3}. \qquad (25)$$

where the level density parameter a is a function of the nucleon effective mass m^* at $T = 0$ MeV with $k = k_F$. By using equation (24) the internal energy of the system at temperature T is defined by[44]

$$F = E_{T=0} - \frac{T^2}{6}\left(\frac{2m^*}{\hbar^2} \right)\left(\frac{3\pi^2}{2} \right)^{1/3} \rho^{-2/3}, \qquad (26)$$

where m^* is the effective mass of the nucleon at zero temperature with $k = k_F$, defined in Eq. (7). It should be

pointed out that the same expressions are obtained for zero range forces[45]. In fact they reflect a general property of the Landau theory of normal Fermi liquids.

2. Results and Discussion

2.1. The Symmetric and Pure Neutron Matter

2.1.1. The Single Particle Energy

In this section we present the results for the single particle energies which is calculating using Equation (2). More discussion can be read in[46]. **Figure 1** shows the dependence of the single particle energy on the momentum k up to $k_{fit} = 1.6 k_F$ for symmetric nuclear matter using the CD-Bonn potential (solid curve), the Argonne V_{18} potential (dashed-double dot curve), the Nijm-I potential (dotted curve), the Nijm-II potential (dashed curve) and the Reid 93 potential (dashed-dot curve) at the normal saturation density $\rho_0 = 0.16$ fm^{-3} in terms of Fermi momentum, $k_F = 1.333$ fm^{-1}. Left panel for conventional choice, right panel for continuous choice. We observe that the results of all potentials are close to each other in the conventional choice and at high momentum after k = k_F the results of all potentials come together, this means that the effect of the potential disappear at values above Fermi momentum k_F. In the continuous choice we note that the CD-Bonn and Nijm-I (non-local) potentials are more attractive than the Argonne V_{18}, the Nijm-II and the Reid 93 (local) potentials and the difference between the potentials continues even at high momentum k, this means that the effect of the potential continues at values above k_F.

If we compare the results we note that, one finds that the single particle energies are more attractive in the continuous choice than those in the conventional choice.
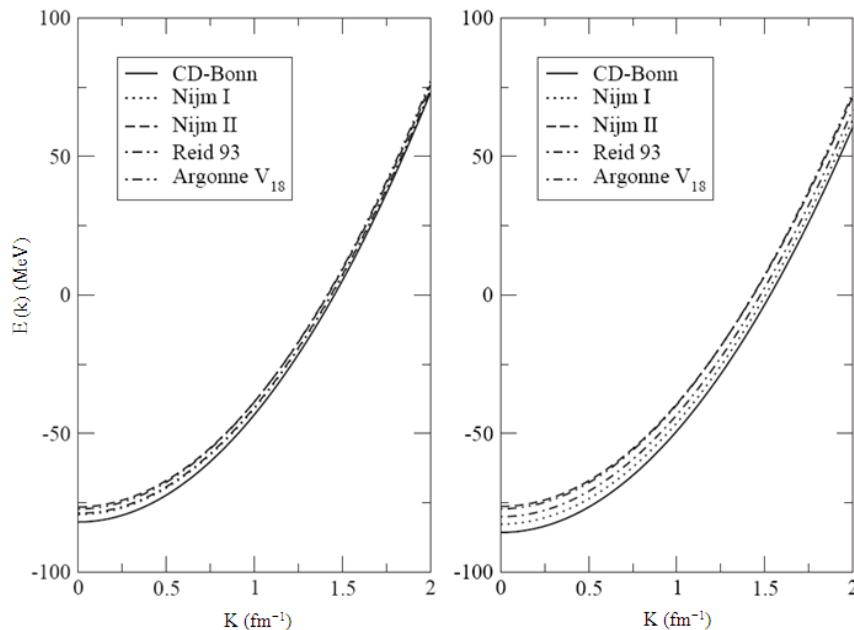

Figure 1. The single particle energy within BHF approach using modern nucleon-nucleon potentials. The left panel represents the results with conventional choice and the right panel with the continuous choice for the auxiliary potential at the normal Fermi momentum $k_F = 1.333$fm^{-1}
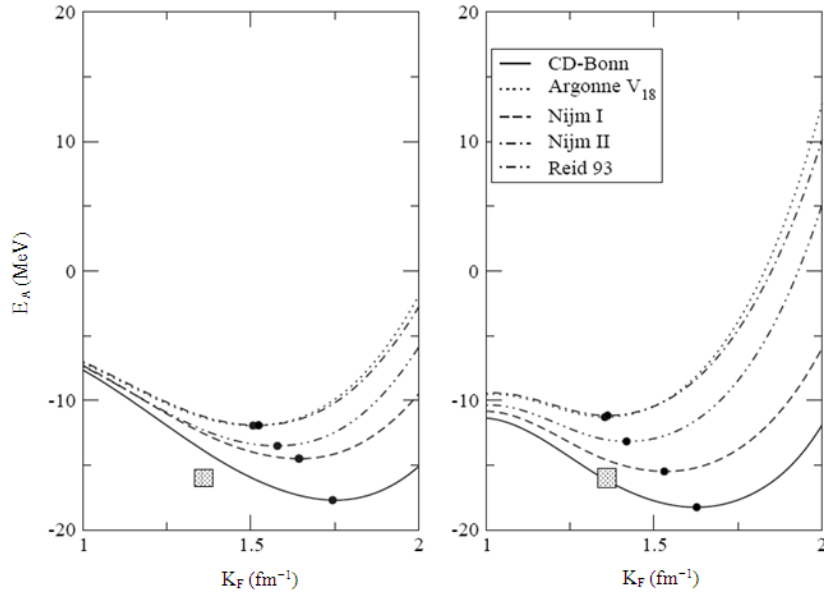
Figure 2. The binding energy per nucleon calculated for symmetric nuclear matter as a function of the Fermi momentum k_F within BHF approach using modern nucleon-nucleon potentials. The left panel represents the results with conventional choice and the right panel with the continuous choice for the auxiliary potential. The solid points are the saturation points and the big square indicates the empirical saturation area

This reflects the fact that the effective interaction is more attractive between nucleons in the continuous choice than the conventional choice. From **Fig. 1** one can also see that the BHF single particle energies have a simple parabolic shape as a function of the momentum for all the interactions. So, one uses a parametrization of the single particle energies in terms of an effective mass using Eq. (7).

Finally we want to stress that, despite the parabolic approximation is not accurate[47] and we use a not so large cutoff for the single particle momentum, we believe that the differences in the results for various NN interactions, obtained within the same approximation scheme, are sensible and meaningful.

2.2. The Nuclear Matter Binding Energy

We present the results of the non-relativistic BHF calculations in **Fig. 2** obtained with different modern NN potentials. The energy per particle E_A in MeV is plotted against the density ρ in terms of Fermi momentum k_F in fm^{-1}, for symmetric nuclear matter using different potentials, the CD-Bonn potential (solid line), the three Nijmegen potentials, Nijm-I (short dashes), Nijm-II (double dot-dashed line) and Reid 93 (dot-dashed line) and the Argonne V_{18} potential (dotted line). Left panel is for conventional choice and the right panel is for continuous choice. The solid points indicate the saturation points and the dashed box indicates the empirical saturation one. One observes from the figure that the binding energy per nucleon, first decreases with increasing k_F, until it reaches the minimum (saturation) point then it increases with increasing the Fermi momentum k_F. The continuous choice leads to an enhancement of correlation effects in the medium and tends to predict larger binding energies for nuclear matter than the conventional choice.

It is found that our calculations lead to results for saturation points, which lie along a line (Coester line) shifted with respect to the phenomenological saturation point (ρ_0 = 0.16 fm^{-3}; E_A = -16MeV). One can see that the continuous choice leads to an enhancement of correlation effects in the medium and tends to predict larger binding energies for nuclear matter than the conventional choice. In the continuous choice that line is close to the empirical data than the conventional choice. So, we can say that our results confirm the concept of a "line", density and energy of the various saturation points being strongly linearly correlated, where that be consistent with the results in Refs.[36, 48]. The saturation points for our results are presented in **Table 1**.

A very important source for the origin of the two-body correlations is the tensor force, which for example, describes the scattering of a proton-neutron pair, which originally is in a relative $^3S_1$ state with momentum below k_F, into a $^3D_1$ state above the Fermi sea. A measure of the strength of the tensor force is expressed in term of the D-state probability P_D obtained for the deuteron[48, 49]. We also observe from **Table 1** that the continuous choice in the Nijm-II potential and Argonne V_{18} potential obey approximately the correct Fermi momentum saturation point but at low binding energy per nucleon. The continuous choice in the Nijm-I potential obeys approximately the correct binding energy per nucleon but at high Fermi momentum. The CD-Bonn potential leads to strong over-binding and too high saturation density than the others, because it contains a weak tensor force. It looks that any increase of the non-locality would improve the fitting of binding energy of nuclear matter, but shifts the saturation point to higher density and binding energy.

In **Fig. 3**, we plot, for comparison also, the energy per particle as a function of Fermi momentum k_F using the continuous choice for the single particle auxiliary potential with the results obtained with the T-matrix and T-matrix

+3BF method with CD-Bonn potential by Somua and Bozek[50] and with BHF +3BF using both CD-Bonn and Argonne V_{18} potentials by Baldo and Shaban[51]. There is another method can be used to enhance the present results if one goes beyond BHF approach.

In **Fig. 4**, the energy per particle E_A is plotted against Fermi momentum k_F, for pure neutron matter using different potentials. Left panel is for conventional choice, right panel is for continuous choice. We compare the results by CD-Bonn +3BF and V_{18}+3BF. The pure neutron matter EoS is unbound with the energy per nucleon rising approximately monotonically with increasing the Fermi momentum, which is in agreement with most of the many-body calculations. We note that the differences between the potentials are small,

because the main source of differences among the potentials is in the strength of the tensor force, which is mostly reflected in the (T = 0) $^3S_1$-$^3D_1$ coupled states. In pure neutron matter (T = 1), however, this partial wave does not contribute.

Only T=1 states contribute to the energy of pure neutron matter while both isospin states contribute to the energy of symmetric nuclear matter, if major T = 0 partial waves become increasingly repulsive at short distances. It is possible for the energy of symmetric nuclear matter to grow at a faster rate and eventually approach the neutron matter EoS. This is just what we observe in our model. In the presence of repulsive forces only, symmetric matter would be a more repulsive system than neutron matter (for the same k_F).
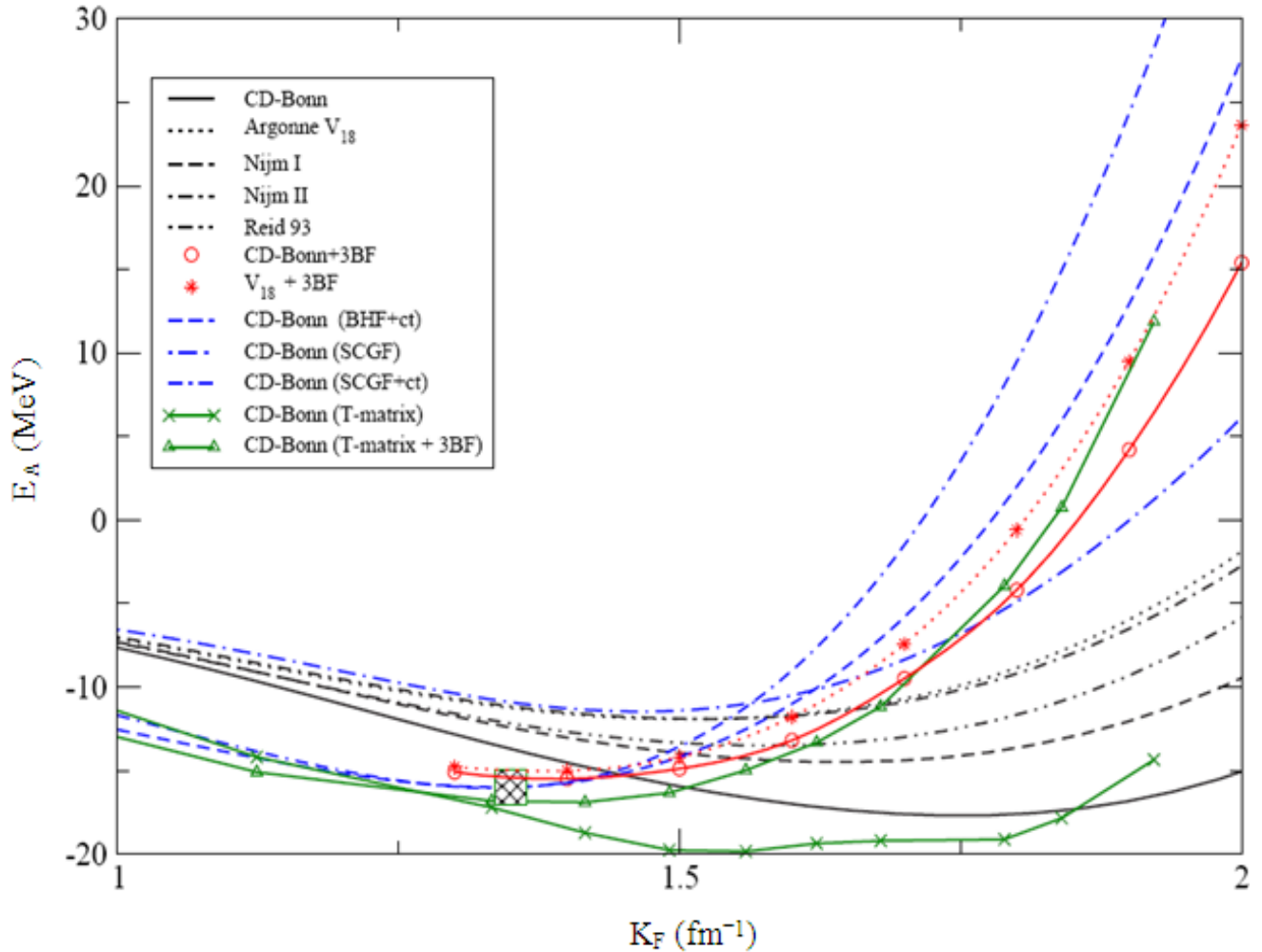

Figure 3. The binding energy per nucleon calculated for symmetric nuclear matter as a function of the Fermi momentum k_F within BHF approach using modern nucleon-nucleon potentials. All the results are calculated with the continuous choice for the auxiliary potential and compared with other approaches, see the text for details. The big square indicates the empirical saturation area
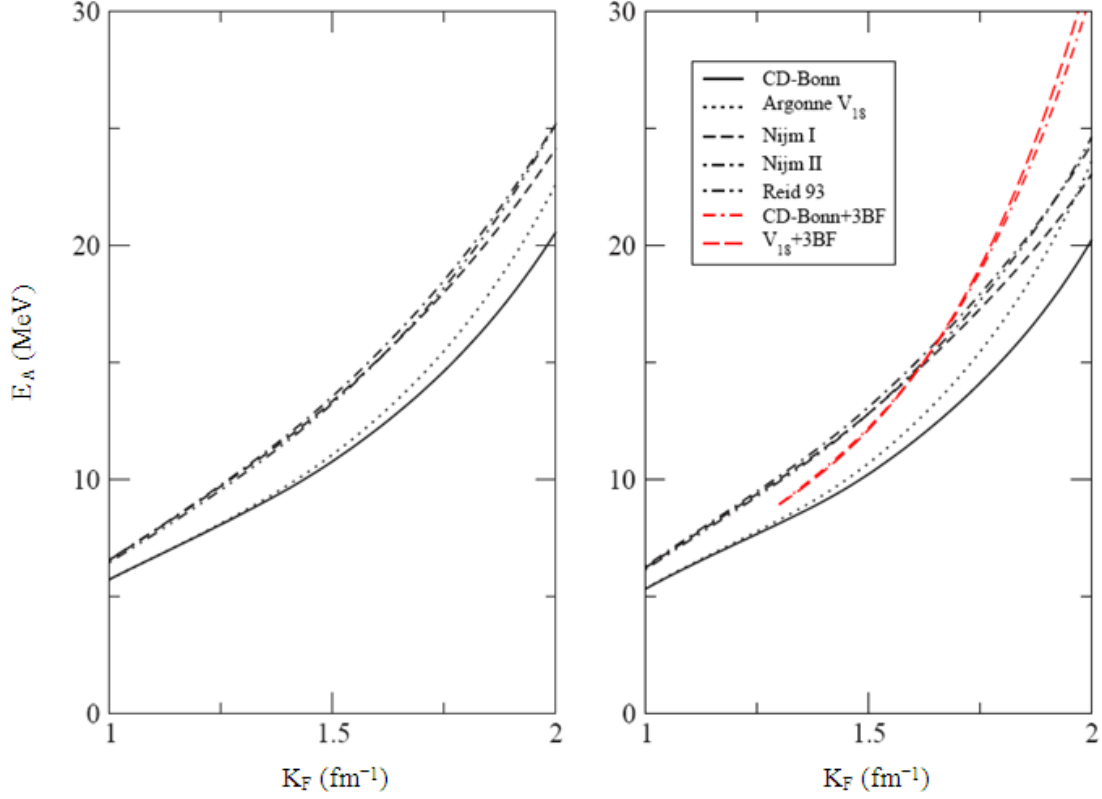
Figure 4. The binding energy per nucleon calculated for pure neutron matter as a function of the Fermi momentum k_F within BHF approach using modern nucleon-nucleon potentials. The left panel represents the results with conventional choice and the right panel with the continuous choice for the auxiliary potential

Table 1.   Summary of the main features of the nuclear matter that be extracted from the equation of state at saturation points. These values are the Fermi momentum k_F^0, saturation energy E_A, symmetry energy E_{sym}, incompressibility K and effective mass m*/m. All results are calculated within BHF approach using the conventional (first group) and continuous (second group) choice for the auxiliary potential

	Conventional choice				
	k_F^0 (fm−1)	-EA (MeV)	E_{sym} MeV	K (MeV)	m*/m
CD-Bonn	1.743	17.70	32.24	208.83	0.566
Arg. V18	1.506	11.94	23.05	137.42	0.632
NijmI	1.643	14.50	30.40	156.38	0.566
NijmII	1.522	11.92	25.89	136.10	0.634
Reid 93	1.578	13.51	28.08	148.18	0.618
	Continuous choice				
CD-Bonn	1.627	18.25	30.23	180.23	0.602
Arg. V18	1.353	11.29	20.11	189.51	0.681
NijmI	1.530	15.49	28.84	148.51	0.639
NijmII	1.361	11.17	22.16	182.94	0.682
Reid 93	1.418	13.17	24.60	121.55	0.664

2.3. Symmetry Energy

The neutron matter EoS combined with that of symmetric nuclear matter provides us with information on the isospin effects[10], in particular on the symmetry energy. The energy per nucleon for nuclear matter is a function of the density ρ and the asymmetry parameter α. Hence, using Taylor's expansion and ignoring higher order terms:

$$E_A(\rho, \alpha) = E_A(\rho, 0) + E_{sym}\, \alpha^2 + O(\alpha^4) + \ldots \quad (27)$$

The symmetry energy of nuclear matter is defined as a second derivative of energy per nucleon E_A with respect to the asymmetry parameter α as follows:

$$E_{sym}(\rho) = \frac{1}{2}\left[\frac{\partial^2 E_A(\rho,\alpha)}{\partial \alpha^2}\right]_{\alpha=0} \quad (28)$$

where, we introduced the asymmetry parameter:

$$\alpha = \frac{\rho_n - \rho_p}{\rho} \quad (29)$$

Both ρ_n and ρ_p are the neutron and proton densities in Asymmetric Nuclear Matter (ANM) and $\rho = \rho_n + \rho_p$ is the total density of asymmetric nuclear matter. It is well established[33, 34, 52] that the binding energy per nucleon E_A fulfills the simple a^2-law not only for a«1 as assumed in the empirical nuclear mass formula[53], but also in the whole asymmetry range. The a^2-law of the EoS of ANM at any isospin asymmetry leads to two important consequences.

First, it indicates that the EoS of ASM at any isospin asymmetry is determined completely by the EoS of SNM and the symmetry energy.

Second, the above α^2-law implies that the difference of the neutron and proton chemical potentials in β-stable neutron

star is determined by the symmetry energy in an explicit way: μ_n-μ_p = 4aE_{sym}[34] and thus the symmetry energy plays a crucial role in predicting the composition of neutron stars.

The results of our calculation for the symmetry energy as a function of baryonic density in terms of the Fermi momentum k_F, Eq.28 are depicted in **Fig. 5**. Also the values of symmetry energy at saturation points are listed in **Table 1**. We observe that the symmetry energy first increases with increasing the Fermi momentum kF until it reaches a maximum value then it decreases with increasing k_F.

In **Table 2** we present the Fermi momentum at which the symmetry energy takes maximum value k_{Fmax} and it reaches zero kFC (critical Fermi momentum) for various potentials. At high k_F the symmetry energy can take negative values, this occurred because at high k_F the EoS for symmetric nuclear matter increases more rapidly and in some potentials increase more than the EoS for pure neutron matter. This means that pure neutron matter system becomes more stable than symmetric matter, a phenomenon referred to as isospin

separation instability[54].

2.4. Asymmetric Nuclear Matter

2.4.1. The Binding Energy

Figure 6 shows the energy per nucleon as a function of the density ρ in asymmetric nuclear matter for various values of the asymmetry parameter a. In order to establish the importance of the hole-hole term in the calculated binding energy we have compared BHF calculations (which ignore the hole-hole term) with SCGF, which includes the hole-hole term. As expected, the hh term gives a repulsive contribution to the EoS of asymmetric nuclear matter. This contribution becomes stronger by increasing the density and makes the EoS at high density much stiffer. As the density increases the phase space for the hole-hole propagator is no longer negligible, resulting in an enhanced repulsive effect on the total energy.
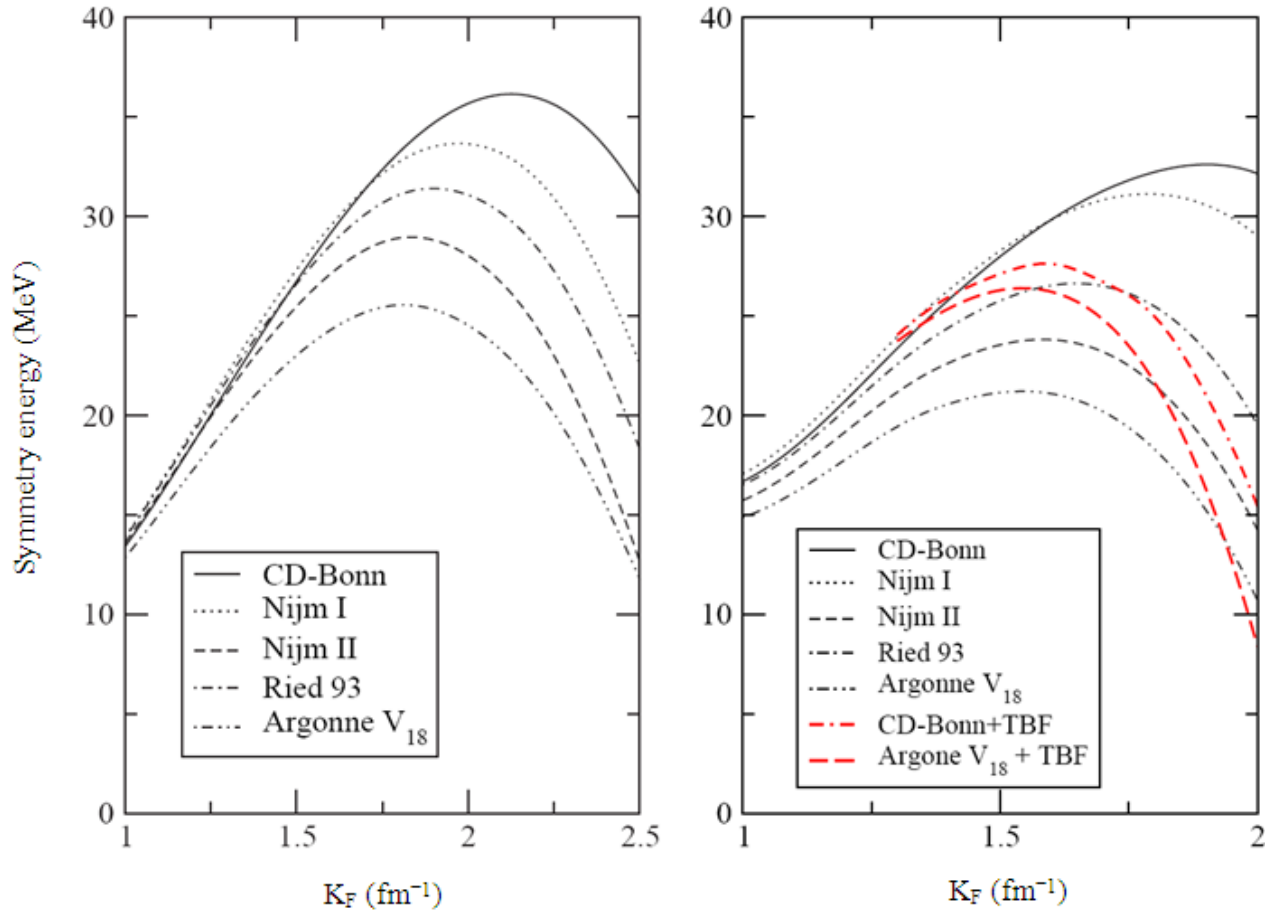

Figure 5. The symmetry energy obtained from Equation (28) as a function of the Fermi momentum k_F. The left panel represents conventional choice and the right panel with the continuous choice for the auxiliary potential
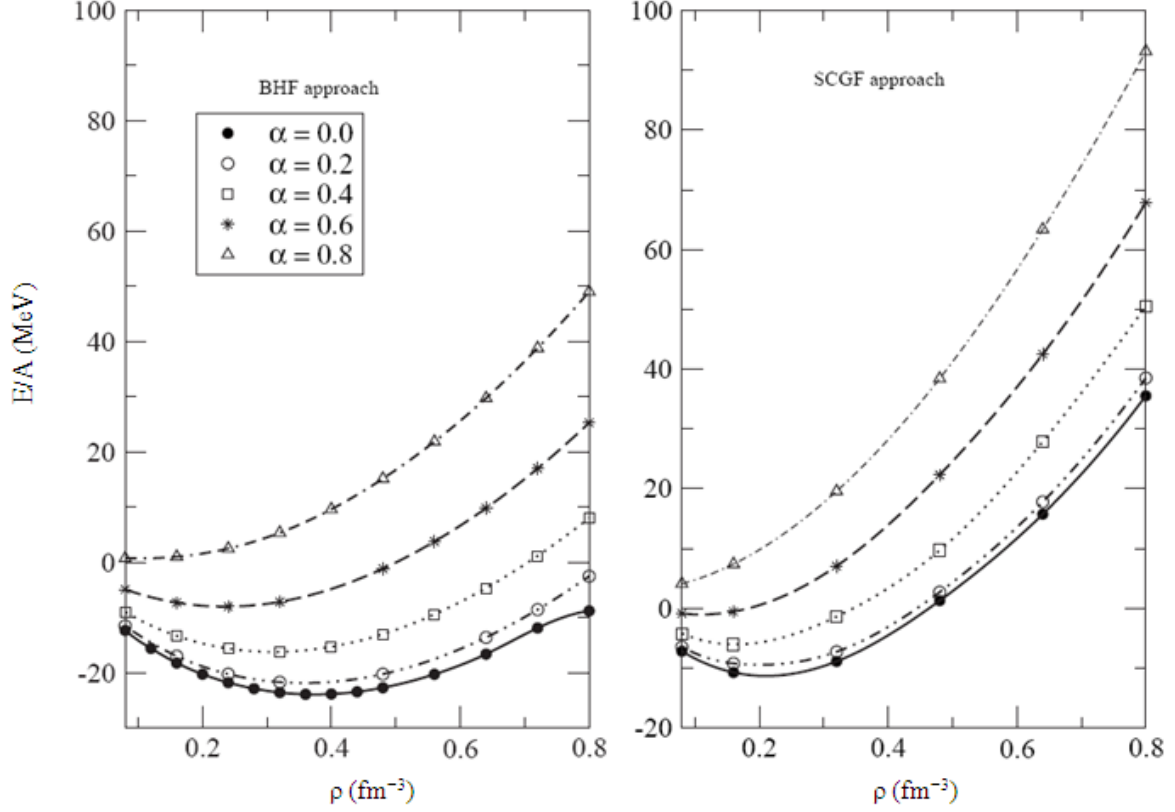
Figure 6. The energy per nucleon for asymmetric nuclear matter as a function of density for various values of the asymmetry parameter α. The predictions are obtained from the BHF (left panel) and the SCGF (right panel) approaches

The additional repulsion from the hh improves greatly the predicted saturation density of cold symmetric nuclear matter. As the neutron density increases (the total density remaining constant), the EoS becomes more and more repulsive. From the figure one notices that, the saturation densities of asymmetric nuclear matter depend on the asymmetric parameter α and the saturation points shift to lower densities. In addition the instability of nuclear matter decreases with increasing asymmetry parameter α, (or decreasing proton fraction).

Table 2. The values of the Fermi momentum that the symmetry energy takes a maximum value k_{Fmax} and it reaches zero at k_{FC} in units of fm^{-1} for the various potentials

	k_{Fmax}(conv)	k_{FC}	k_{Fmax}(cont	k_{FC}
CD-Bonn	2.1	Above 3	1.9	2.6
Arg. V18	1.8	2.8	1.5	2.2
NijmI	1.9	2.8	1.8	2.5
NijmII	1.8	2.7	1.6	2.2
Reid 93	1.9	2.8	1.6	2.3

Table 3. The difference between neutron and proton chemical potentials are reported for two approximations used in the present work for CD-Bonn potential at asymmetry papameter α = 0.8. All chemical potentials difference are given in MeV

Method	BHF	SCGF
Density ρ	$4\,\alpha\,E_{sym}$	$4\,\alpha\,E_{sym}$
0.08	65.3	56.4
0.16	96.3	90.6
0.32	145.0	142.4
0.48	189.5	185.9

The EoS in the case of asymmetric nuclear matter was studied in more details in Ref.[33].

2.5. The Symmetry Energy and its Relation with the Chemical Potential

Within the parabolic approximation (Eq. 16) in[34] one can obtain the neutron and proton chemical potentials in asymmetric nuclear matter in the following way[55, 56]:

$$\mu_{n,p}(\rho,\alpha) \approx \mu_{n,p}(\rho,\alpha=0)$$
$$-\left(\alpha^2 \mp 2\alpha - \alpha^2\rho\frac{\partial}{\partial\rho}\right)E_{sym}(\rho) \tag{30}$$

where, the minus sign is for neutrons and the plus sign for protons and in particular:

$$\mu_n(\rho,\alpha) - \mu_p(\rho,\alpha) = 4\alpha E_{sym}(\rho) \tag{31}$$

The nucleon chemical potential difference can be calculated once we have the coefficient of symmetry energy from Eq. (31). In **Table 3** the shift between neutron and proton chemical potentials μ_n-μ_p as function of the density for BHF and SCGF approaches using CD-Bonn potential at asymmetry parameter α = 0.8. Reveals that there is a negligible difference between the BHF and the SCGF approximations. This means that the hh ladder brought about negligible contributions to the chemical potential difference specially at high density.

2.6. Properties of Asymmetric Nuclear Matter

2.6.1. How to Reproduce the Empirical Saturation Point

All results of calculations, which refer to realistic NN interactions, have been obtained using the CD-Bonn[7] interaction. This includes all BHF and SCGF calculations. Also the evaluation of V_{lowk} has been based on the proton-neutron part of CD-Bonn. The Skyrme Hartree-Fock calculations have been done using the parameterization SLy4 and for the relativistic mean-field calculation the parameterization for DDRMF in[57] has been used.

First let us turn to the binding energy of symmetric nuclear matter, which are displayed in **Fig. 7**. Compared to other realistic NN interactions the CD-Bonn potential, which we have chosen here is a rather soft NN interaction with a weak tensor force. This is indicated by the results for the saturation point of symmetric nuclear matter as obtained in the BHF approximation (the minimum of the dashed black line in **Fig. 7** and data in **Table 4**). The saturation density is larger than twice the empirical value and the calculated energy is well below, which means that the CD-Bonn result is located in the large binding energy high density part of the Coester band[1].

In order to reproduce the empirical saturation point of symmetric nuclear we have added an isoscalar interaction term as defined in Eq. (21) choosing a value for $\delta = 0.5$ and fitting the parameters t_0 and t_3. The results for these fitting parameters are listed in **Table 5** and the corresponding energy versus density curves are displayed in **Fig. 7**.

2.7. The Nuclear Compressibility Modulus or the Incompressibility

The results for the calculated saturation points in **Table 4** are supplemented by the corresponding values for the nuclear compressibility modulus:

$$K = 9\rho_0^2 \frac{\partial^2 (E/A)}{\partial \rho^2}\bigg|_{\rho=\rho_0} \tag{32}$$

Table 4. Properties of symmetric nuclear matter are compared for Skyrme SLy4, DDRMF, BHF, SCGF and V_{lowk}. The results, which are listed in the columns labeled with +ct are obtained employing the additional contact interaction of Eq. (21) with parameters as listed in **Table 5**. The quantities listed include the saturation density ρ_0, the binding energy at saturation E/A, the compressibility modulus K and the symmetry energy at saturation density $a_S (\rho_0)$

	ρ_0 (fm^{-3})	$E/A(\rho_0)$ (MeV)	K (MeV)	$a_S (\rho_0)$ (MeV)
Sly4	0.160	-15.97	230	32.0
DDRMF	0.178	-16.3	337	32.1
BHF	0.374	-23.97	286	51.4
BHF+ct	0.161	-16.0	214	31.9
SCGF	0.212	-11.5	203	34.0
SCGF+ct	0.160	-16.1	270	28.3
V_{lowk}+ct	0.160	-16.0	258	21.7

Table 5. Parameters t_0 and t_3 defining the contact interaction of Equation (21) as obtained for the fit to the saturation point $\rho = 0.16$ fm^{-3} and E/A = -16.0 MeV at $\delta = 0.5$ for various realistic approaches

	BHF	SCGF	V_{lowk}
t_0 (MeV fm^3)	-153	-311	-438.1
t_3 (MeV fm$^{3+3\delta}$)	2720	3670	6248

This nuclear compressibility, which is calculated at the saturation density ρ_0, together with the increase of energy at large density displayed in **Fig. 7** characterize the stiffness of the EoS of symmetric nuclear matter.
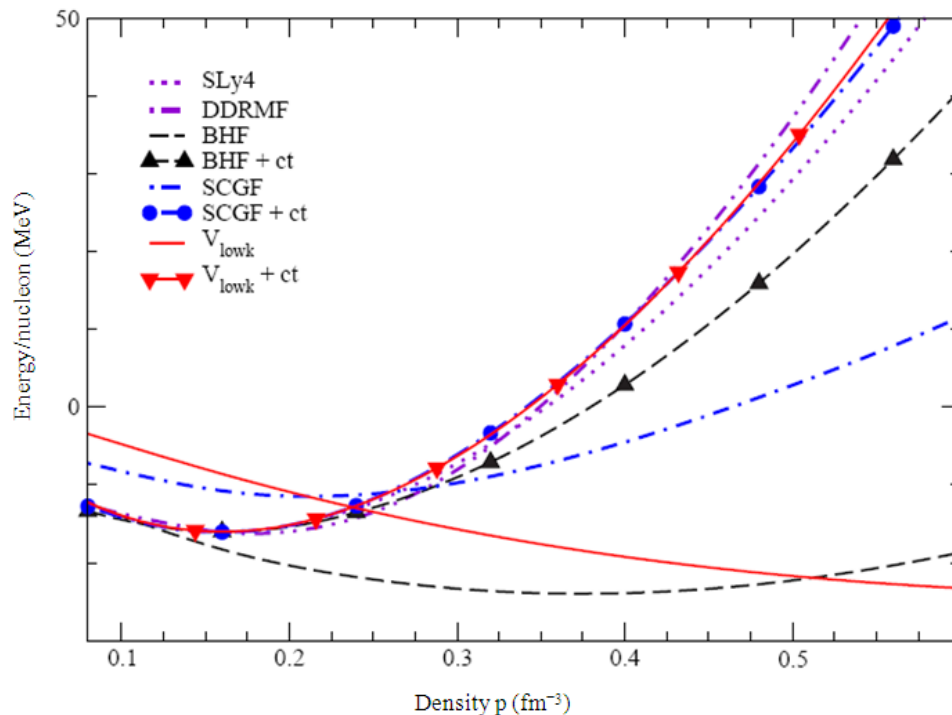

Figure 7. (Color online) Comparison of binding energy per nucleon of symmetric nuclear matter as obtained from Skyrme SLy4, DDRMF, BHF, SCGF and V_{lowk}. Results of approaches based on realistic NN interactions are also compared with an additional contact interaction of the form displayed in Eq. (21)

Comparing the different approaches we find that the relativistic features included in the DDRMF approach lead to the stiffer EoS around the saturation density as well as at higher densities. The SCGF and the V_{lowk} calculations yield rather similar results after the contact terms are included, which are a little bit softer than the DDRMF results and characterized by a compression modulus of 270 MeV and 258 MeV for SCGF and V_{lowk}, respectively. At higher densities the results are also very close to those obtained for the Skyrme Hartree-Fock using SLy4. Note, however, that SLy4 yields a rather low value for K as compared to the SCGF and V_{lowk} calculations. The softest EoS for symmetric matter among those approaches which fit the empirical saturation point is provided by the BHF approximation.

2.8. The Nuclear Symmetry Energy

Table 5 also displays results for the symmetry energy:

$$a_S(\rho) = \left.\frac{\partial(E/A)}{\partial\alpha^2}\right|_\rho , \quad \alpha = \frac{N-Z}{A} = 1 - 2Y_p \quad (33)$$

Evaluated for each approach at the corresponding saturation density ρ_0. The two phenomenological approaches SLy4 and DDRMF yield results which are in the range of the experimental value of 32±1 MeV. Also the BHF and SCGF approach lead to results which are rather close to the empirical value, if the contact term has been added. The BHF and SCGF calculations without the contact term lead to non-realistic values for $a_S(\rho_0)$ since these values are calculated at the corresponding saturation densities, which are larger than the empirical saturation density.

The symmetry energy calculated in the SCGF approach is slightly smaller than the one obtained from the BHF approximation. This is valid for all densities under consideration (**Fig. 8**). This difference can easily be explained: As we already mentioned above, the contribution of the hole-hole terms is repulsive, which leads to larger energies for SCGF as compared to BHF for all densities in symmetric nuclear matter (**Fig. 7**) as well as in pure neutron matter (**Fig. 9**). Since, however, the contribution of ladder diagrams is larger in the proton-neutron interaction (due to the strong tensor terms in the $^3S_1$-$^3D_1$ partial wave) than in the neutron-neutron interaction, this repulsive effect is stronger in symmetric nuclear matter than in neutron enriched matter. Therefore the symmetry energy calculated in SCGF is slightly smaller if the hole-hole terms are included in SCGF[58].
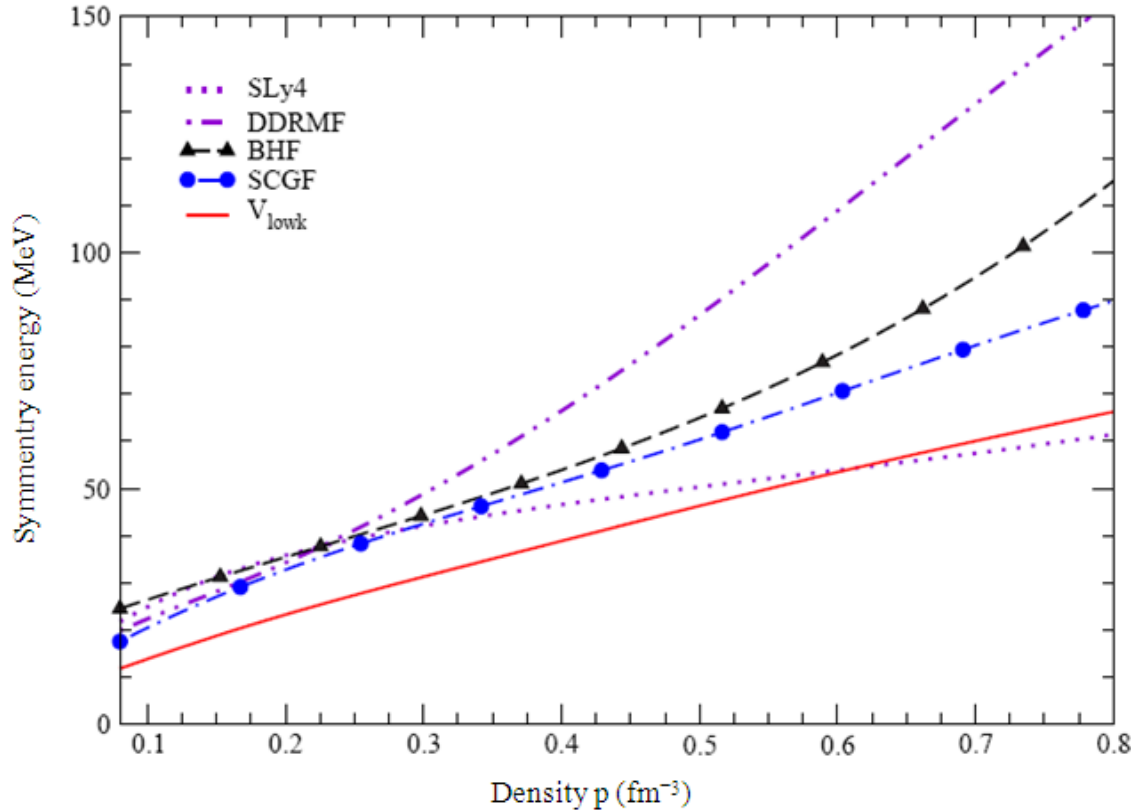

Figure 8. (Color online) Comparison of the symmetry energy $a_S(\rho)$ as a function of density ρ as obtained from Skyrme SLy4, DDRMF, BHF, SCGF and V_{lowk} approaches
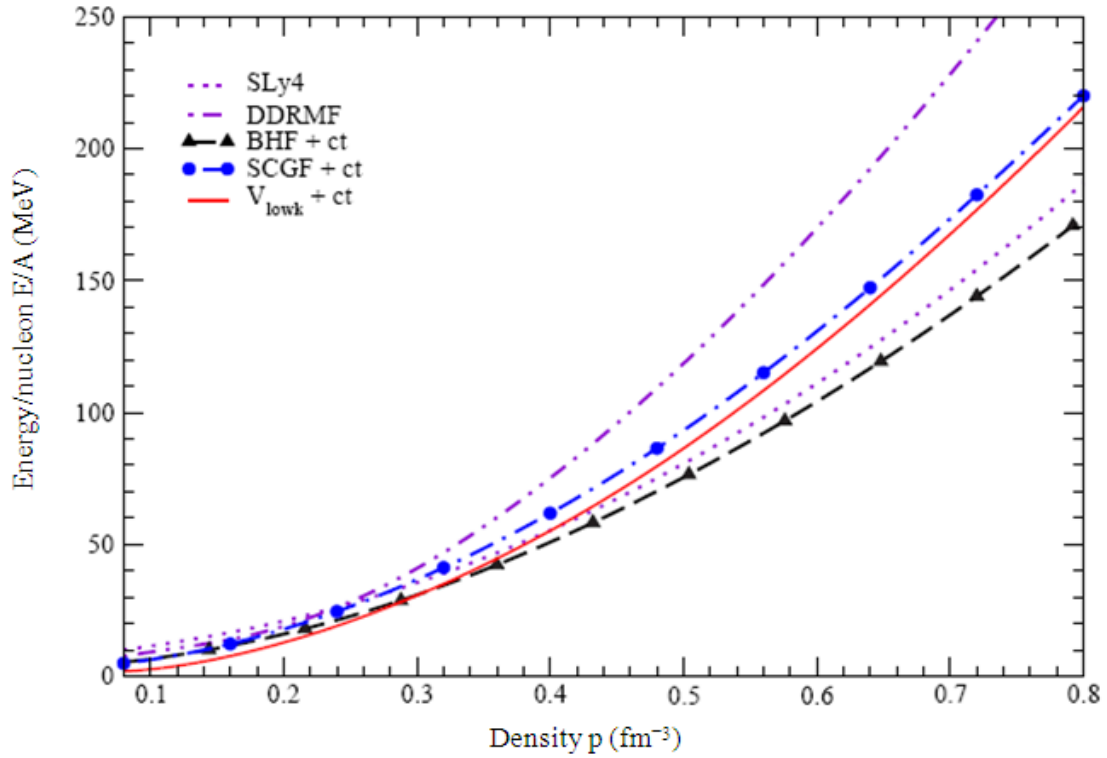
Figure 9. (Color online) Energy per nucleon of pure neutron matter as a function of density as obtained from Skyrme SLy4, DDRMF, BHF, SCGF and V_{lowk} approaches
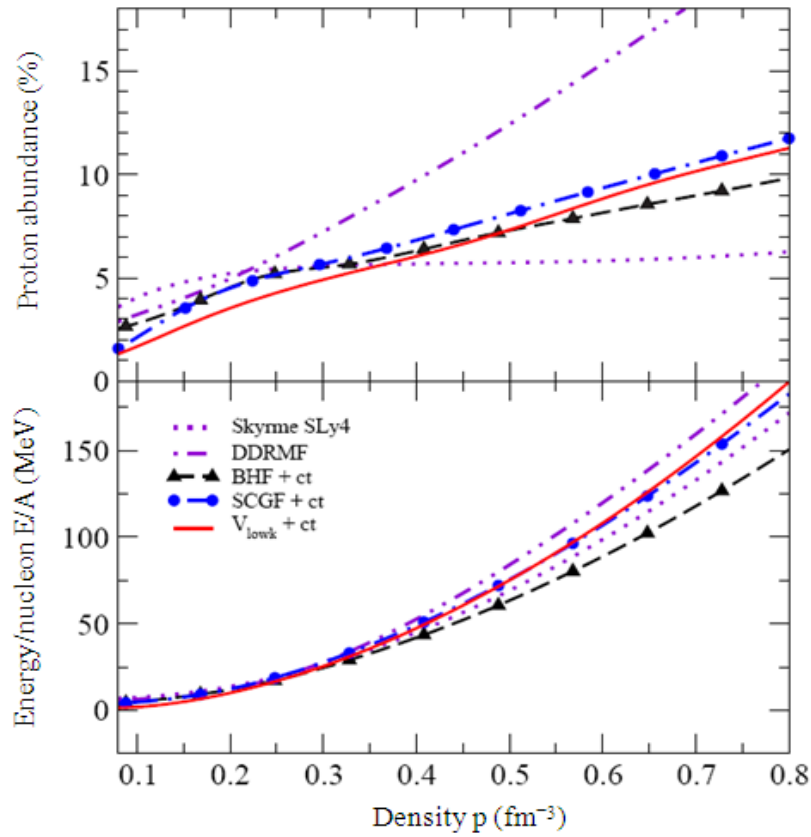

Figure 10. (Color online) Results for a system of infinite matter consisting of protons, neutrons and electrons in β-equilibrium. The upper panel show the proton abundances and the lower panel displays the energy per nucleon as a function of density using the various approximation schemes discussed in the text

The symmetry energy rises as a function of density for all approaches considered. Note, however, that the two phenomenological approaches Skyrme Hartree-Fock using SLy4 and DDRMF provide rather different predictions at high densities although the symmetry energy at normal density is identical. The relativistic approach predicts symmetry energies for high densities, which are well above all those derived from the microscopic calculations, while the Skyrme interaction yields a symmetry energy which is even below the V_{lowk} estimate at densities above four times saturation density.

2.9. β-Equilibrium

Rather similar features also observed, when we inspect the properties of nuclear matter in β-equilibrium, neutralizing the charge of the protons by electrons, displayed in Fig. 10. The upper panel of this figure displays the proton abundance $Y_p = Z/A$, which are to some extent related to the symmetry energy: large symmetry energy should correspond to large proton abundances. So the largest proton abundances are predicted within the DDRMF approach. Already at a density around 0.4 fm^{-3} Y_p exceeds the about 10%, which implies that the direct URCA process could be enabled, which should be reflected in a fast cooling of a neutron star.

The V_{lowk} and SCGF approaches lead to similar proton abundances at large densities. This demonstrates that the evaluation of the proton abundance in β-equilibrium cannot directly be deduced from the symmetry energy, since the former observable is derived from proton and neutron energies at large asymmetries (Z<<N), whereas the symmetry energy is calculated from the second derivative at N = Z (Eq. (28)). The BHF approach shows slightly lower values for Y_p at high density, but the results are still in the same range as SCGF and V_{lowk}.

At low densities the Skyrme HF approach yields large proton fractions as compared to the results of the other calculations. Large proton fractions at low densities tend to enhance density inhomogeneities and thus favor the existence of a large variety of pasta structures. Therefore the Skyrme HF (Sly4) and the DDRMF approach, which have been explored in detail in[57, 59], should favor the formation of pasta structures as compared to the microscopic approaches. Comparing the energies of matter in β-equilibrium derived from the various approaches as a function of density (**Fig. 10**, lower panel) we find the same trends as in the case of pure neutron matter displayed in **Fig. 9**.

The equation of state of nuclear matter in β-equilibrium is the main input to predict mass and radii of neutron stars. A stiffer equation of state supports a larger maximum mass and a lower central density. In addition a thicker crust is found for the stiffer equation of state[60].

2.10. The Isovector Effective Mass

Another important information for the evaluation of dynamical features of matter in neutron stars is the density of states, which can be characterized by an effective mass. The term effective mass is used in various connections in many-body physics. This includes the effective masses, which express the non-locality of the self-energy in space and time, which corresponds to a momentum and energy dependence. Such effective masses for protons and neutrons determined for nuclear matter in β-equilibrium are displayed in **Fig. 11** as a function of density considering non-relativistic approximation schemes.

It is a general feature of all approaches considered that the effective masses for protons as well as neutrons decrease with increasing density. However, there is a striking difference between the phenomenological Skyrme approximation and the BHF and V_{lowk} approach, which are based on realistic NN interactions: The effective mass for protons is smaller than the corresponding one for neutrons in neutron rich matter for the calculations using realistic interactions, while it is opposite applying the Skyrme parameterization. In fact, if we define the effective masses for protons m m_p^* and neutrons m_n^* in terms of isoscalar m_S^* and isovector masses m_V^* by:

$$\frac{1}{m_n^*} = \frac{1}{m_S^*} + \alpha\left(\frac{1}{m_S^*} - \frac{1}{m_V^*}\right)$$

$$\frac{1}{m_p^*} = \frac{1}{m_S^*} - \alpha\left(\frac{1}{m_S^*} - \frac{1}{m_V^*}\right) \quad (34)$$

$$\text{with } \alpha = \frac{N-Z}{A},$$

It turns out most of the Skyrme parameterizations yield an effective isovector mass m_V^*, which is even larger than the bare nucleon mass M[61] which implies that it is larger than the effective isoscalar mass m_S^*. This means that the effective mass for neutrons is smaller than the corresponding one for the protons in neutron rich matter (α>0). These Skyrme parameterizations leading to a large effective isovector mass are usually favored as they correspond within the mean-field approach to an enhancement factor k of the Thomas-Reiche-Kuhn sum-rule[62, 63].

Non-relativistic descriptions of nuclear matter, which are based on realistic interactions yield an effective isovector mass m_V^* which is smaller than the corresponding effective isoscalar mass, which leads to a larger effective mass for neutrons than for protons in neutron-rich matter (**Fig. 11**). In order to analyze this finding we inspect the dependence of the nucleon self-energy in the BHF approximation $\sum_i^{BHF}$, defined in Eq. (7), as a function of energy ω and momentum k of the nucleon considered. Following the discussion of Mahaux and Sartor[38] one can define the effective k-mass:

$$\frac{m_k(k)}{M} = \left[1 + \frac{M}{k}\frac{\partial \sum(k,\omega)}{\partial k}\right]^{-1} \quad (35)$$
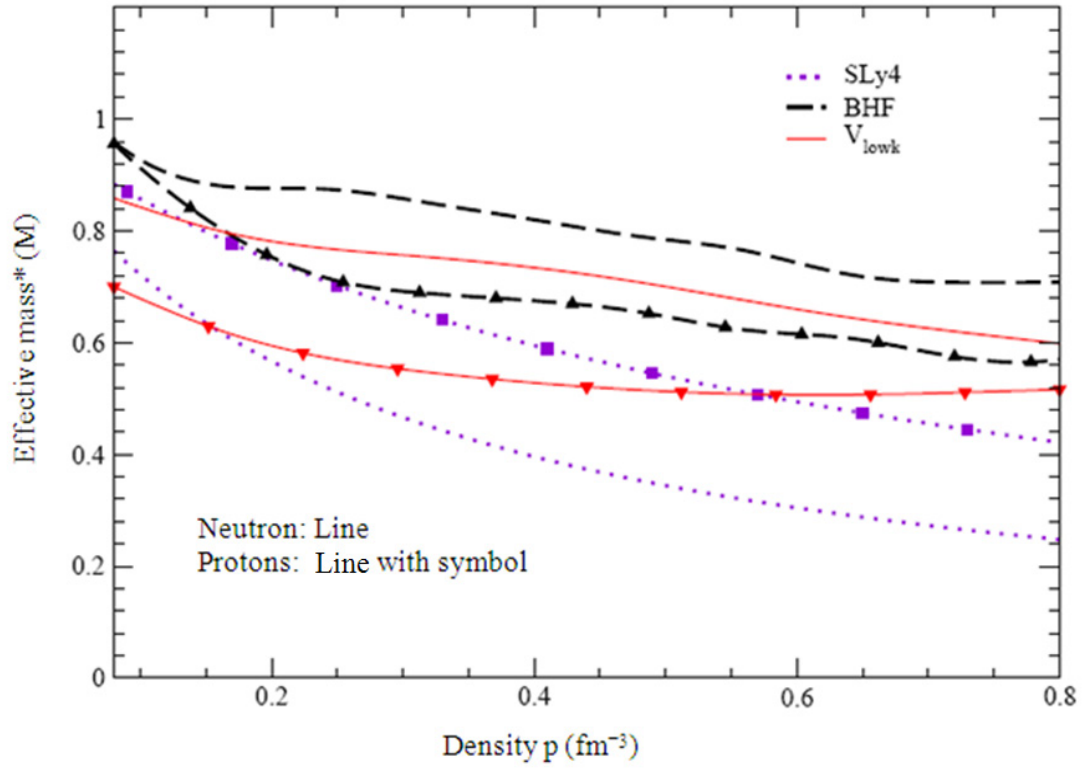
Figure 11. (Color online) Effective masses for protons (lines with symbols) and neutrons (lines without symbols) as obtained for nuclear matter in β-equilibrium using Skyrme HF (SLy4), BHF and V_{lowk} approaches
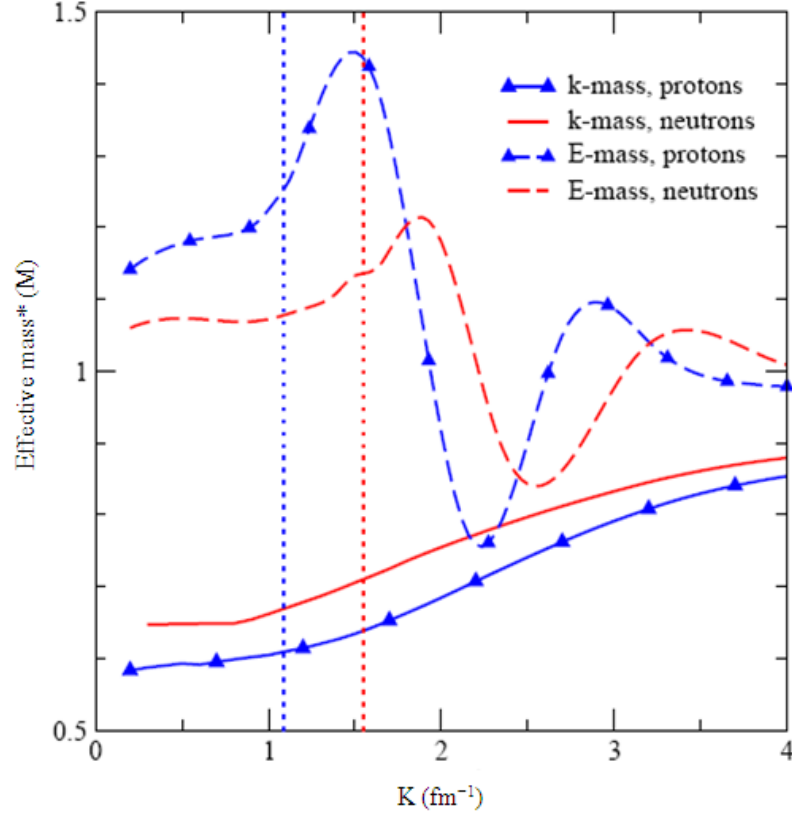

Figure 12. (Color online) Effective k-mass m_k^* k) (solid lines) and effective E-mass m_E^* (k) (dashed lines) for neutrons and protons (lines with symbol) as obtained from the BHF calculations for asymmetric nuclear matter at the density ρ = 0.17 fm^{-3} and a proton abundance of 25%. The Fermi momenta for protons and neutrons are indicated by vertical dotted lines

And the effective E-mass

$$\frac{m_E(\omega)}{M} = \left[1 - \frac{\partial \sum(k,\omega)}{\partial \omega}\right]. \tag{36}$$

The effective mass can then be calculated from the effective k-mass and the effective E-mass by:

$$\frac{m^*(k)}{M} = \frac{m_k^*(k)}{M} \frac{m_E^*(\omega = \varepsilon(k))}{M} \tag{37}$$

Results for the effective k-mass and E-mass as obtained from BHF calculations for asymmetric nuclear matter at a density $\rho = 0.17 \text{ fm}^{-3}$ and a proton abundance Y_p of 25% ($\alpha = 0.5$) are displayed in **Fig. 12**. We notice that the effective k-mass for the protons is significantly below the corresponding value for the neutrons at all momenta. Since the k-masses tend to increase as a function of the nucleon momentum k, the difference in the Fermi momenta for protons and neutrons enhance the difference $m_{k,n}^*(k_{Fn}) - m_{k,p}^*(k_{Fp})$.

The effective k-mass describes the non-locality of the BHF self-energy. This non-locality and thereby also these features of the effective k-mass are rather independent on the realistic interaction used. Furthermore it turns out that the values for the k-mass are essentially identical if one derives them from the nucleon BHF self-energy using the G-matrix or from the bare interaction V or from V_{lowk}[2]. This non-locality of the self-energy is dominated by Fock exchange contribution originating from ρ-exchange. In neutron-rich matter this contribution leads to a stronger depletion for the proton mass than for the neutron mass[4, 64].

Anyway, the enhancement of the effective mass m*, which is due to the effective E-mass in Equation (34) is not strong enough to compensate the effects of the k-mass. Therefore the final effective mass is below the bare mass M and the effective mass for neutrons remains larger than the corresponding one for protons.

2.11. The Symmetry Potential Usym

Regarding $U_{n/p}$ as functions of the asymmetry parameter a, one can easily verify that the following approximate relation applies:

$$U_{n/p}(k,\rho,\alpha) \approx U_{n/p}(k,\rho,\alpha = 0) \pm U_{sym}(k,\rho)\alpha, \tag{38}$$

with the ± referring to neutron/proton, respectively. The difference between the neutron and proton potentials then gives an accurate estimate for the strength of the isovector or symmetry potential in asymmetric nuclear matter, i.e.:

$$U_{sym} = \frac{U_n - U_p}{2\alpha} \tag{39}$$

which is of particular interest and importance for nuclear reactions induced by neutron-rich nuclei. The isovector part of the nucleon potential as a function of nucleon kinetic energy is illustrated in **Fig. 13** at asymmetry parameter a = 0.2 (upper panel) and at a = 0.4 (lower panel). The strength of the isovector nucleon optical potential, i.e., the symmetry or Lane potential[65], can be extracted from Equation (39) at ρ_0. Systematic analysis of a large number of nucleon-nucleus scattering experiments at beam energies below about 100 MeV indicates undoubtedly that the Lane potential decreases approximately linearly with increasing the beam energy E_{kin}, i.e., $U_{Lane} = a - b_{Ekin}$ where $a \approx 22\text{-}34 \text{ MeV}$ and $b \approx 0.1\text{-}0.2$.

Figure 13 shows the theoretical symmetry potentials that have been calculated in both BHF and SCGF approaches in comparison with the Lane potential constrained by the experimental data. The vertical bars are used to indicate the uncertainties of the coefficients a and b. It is seen that the strength of symmetry potential decreases with increasing energy. This trend is in agreement with that extracted from the experimental data. At the saturation density, the nuclear symmetry potential is found to change from positive to negative values at a nucleon kinetic energy of about (200 MeV). This is a very interesting result as it implies that the proton (neutron) feels an attractive (repulsive) symmetry potential at lower energies but a repulsive (attractive) symmetry potential at higher energies in asymmetric nuclear matter. It has been shown that[64] the U_{sym} is almost independent of the isospin asymmetry a within the BHF framework, implying a linear dependence of neutron and proton single-particle potentials on α and providing a microscopic support for the empirical assumption of the Lane potential[65]. Also the present results indicate that the U_{sym} is almost independent of the isospin asymmetry a within the BHF and SCGF approaches.

2.12. Free Energy of the Symmetric Nuclear Matter at Finite Temperatures

Many attempts were made to use the BHF calculations at finite temperature[8, 43, 66, 67]. In Fig. 14, the internal energy *F* of nuclear matter in MeV is plotted against the density ρ in fm^{-3} and the values obtained with the low temperature expansion (26). The results are shown in Fig. 14, for symmetric nuclear matter using different potentials. For both *T* = 8 (upper graph) and *T* = 12 MeV (lower one), for continuous choice. Fig. 14 gives the results obtained using the CD-Bonn potential (solid line), the Nijm1 potential (dashed line) and the Reid 93 potential (dashed–dot line) in comparison with a more elaborate calculation using Argonne V_{14} plus microscopic 3BF[43] (dashed double dotted line). From the plotted figures it is observed that the internal energy first decreases with increasing the density until it reaches a minimum then it increases with increasing the density. Our results are comparable to those obtained in Ref.[43]. The same results have been done using the conventional choice of the auxiliary potential in Ref.[68].
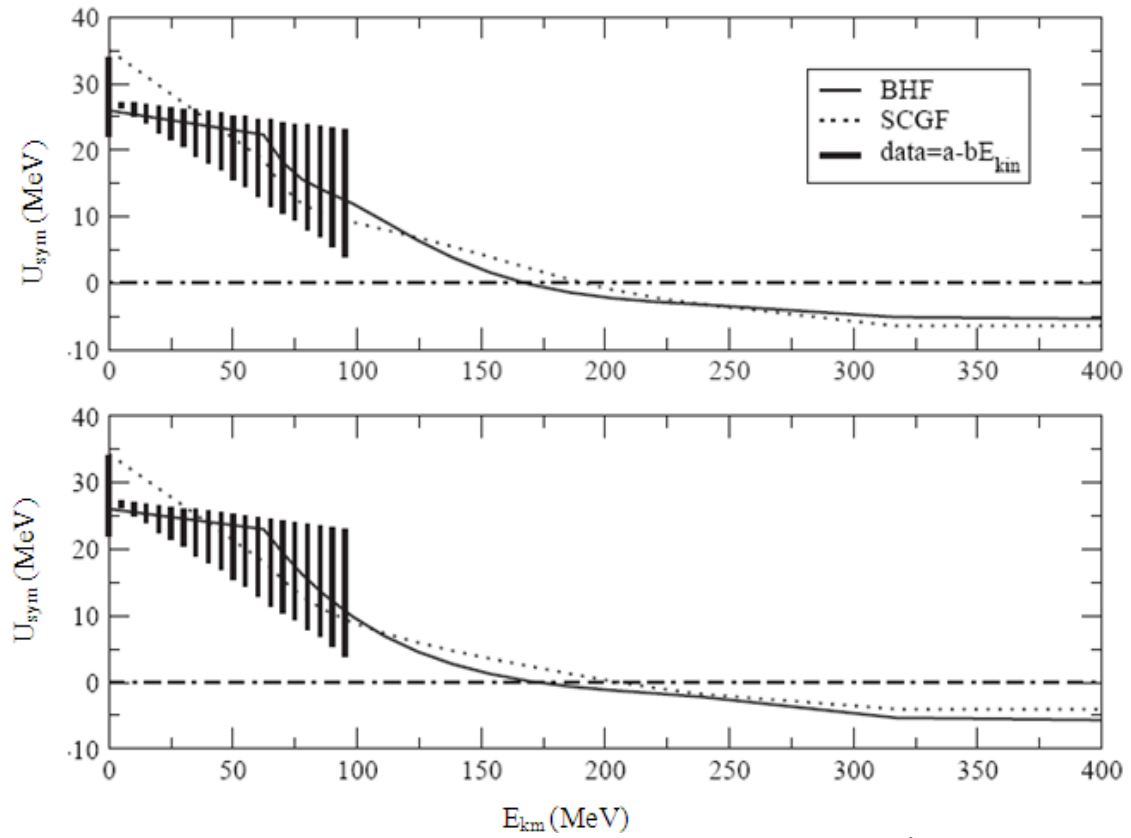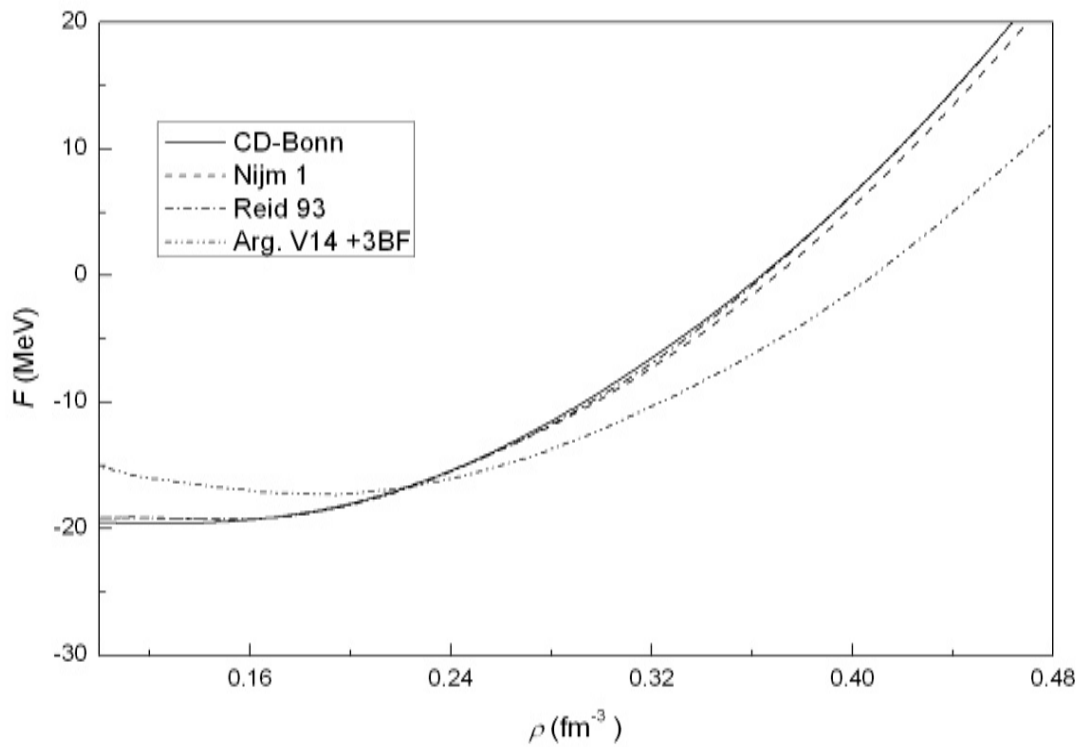
Figure 13. The symmetry potential as a function of the nucleon kinetic energy at nuclear matter density ($\rho = 0.16\,\text{fm}^{-3}$) and at asymmetry parameter $\delta = 0.2$ (upper panel) and at $\delta = 0.4$ (lower panel). The predictions are obtained with the CD-Bonn potential and compared with the empirical information from the nuclear optical potential data (shaded area)
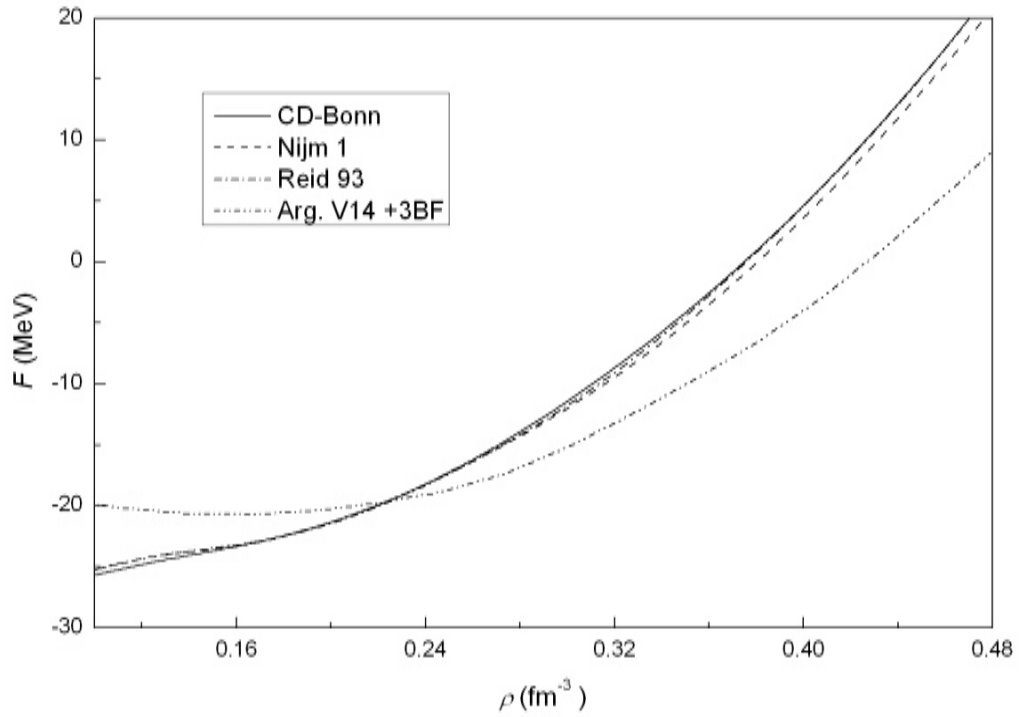
Figure 14. The internal energy at $T = 8$ MeV (upper figure) and $T=12$ MeV (lower one) for symmetric nuclear matter as a function of density using different potentials for continuous choice compared with Argonne V_{14} plus microscopic 3BF by Baldo and Ferreira[43]

3. Conclusions

We have investigated the effect of different modern nucleon-nucleon potentials on the EoS, i.e., the nuclear matter binding energy per nucleon, within BHF approach. It is found that our calculations lead to results, which lie along a line (Coester line) shifted with respect to the phenomenological saturation point ($\rho_0 = 0.16$ fm^{-3}, $E_A = -16$ MeV).

We have reviewed the current status of the Coester line, i.e., the saturation points of nuclear matter obtained within BHF approach using the conventional and continuous choice for the auxiliary potential and employing the modern nucleon-nucleon potentials. It is found that our results confirm the concept of a "line", density and energy of the various saturation points being strongly linearly correlated.

We have presented a microscopic calculation of the equation of state of nuclear matte when protons and neutrons have different Fermi momenta. The techniques to evaluate the single-particle green's function in a Self-Consistent G-matrix approach (SCGF). The continuous choice has been adopted for the auxiliary potential. The single-particle energy is calculated self-consistently using BHF and SCGF approximations. The contribution of the hh terms leads to a repulsive contribution to the single-particle energy which decreases with momentum. The dependence of the EoS on the neutron excess parameter is clearly linear as a function of a^2. The inclusion of the hole-hole ladders and the self-consistent treatment of the Green's function in the

SCGF approach leads to a small reduction of the binding energy per nucleon as compared to the BHF approximation.

Various approaches to the nuclear many-body problem have been investigated to explore their predictions for nuclear matter at high density and large proton-neutron asymmetries. Two of these approaches, the Skyrme Hartree-Fock and the Density Dependent Relativistic Mean Field approach are predominantly of phenomenological origin. Their parameters have been adjusted to reproduce data of finite nuclei. However, the parameters have been selected in such a way that also bulk properties of asymmetric nuclear matter derived from microscopic calculations are reproduced. The other three approaches are based on realistic NN interactions, which fit the NN scattering phase shifts. In these approximation schemes (Brueckner Hartree Fock BHF, Self-consistent Greens Function SCGF and Hartree Fock using a renormalized interaction V_{lowk}) a isoscalar contact interaction has been added to reproduce the empirical saturation point of symmetric nuclear matter.

These various approximation schemes lead to rather similar predictions for the energy per nucleon of symmetric and asymmetric nuclear matter at high densities. In detail one finds that the relativistic DDRMF leads to a rather stiff Equation of State (EoS) for symmetric matter while the BHF approach leads to a relatively soft EoS, a feature which is compensated within the microscopic framework by the repulsive features of the hole-hole ladders included in SCGF. These features are also reflected in the study of nuclear matter

in the β-equilibrium and lead to moderate differences in the predictions for proton abundances and EoS.

More significant differences are observed when we inspect details like the effective masses, in particular the isovector effective mass. In neutron-rich matter the microscopic approaches predict a positive difference between neutron and proton effective masses. This feature can be related to the non-locality of the self-energy induced by one-pion exchange term and is expressed in terms of an effective k-mass.

Also the symmetry potential has been calculated as a function of the nucleon kinetic energy. We observe that the strength of the predicted symmetry potential decreases with energy, a behavior which is consistent with the empirical information. It is interesting to note that at normal density ($\rho = 0.16$ fm^{-3}), the nuclear symmetry potential changes from positive to negative values at nucleon kinetic energy around 200 MeV. More details can be read in Ref.[69].

ACKNOWLEDGMENTS

REFERENCES

[1]   H. Müther and A. Polls, Prog. Part. Nucl. Phys., 45: 243 (2000).

[2]   T. Frick, K. Gad, H. Müther and P. Czerski, Phys. Rev., C 65: 034321, (2002).

[3]   T. Frick, Kh.S.A. Hassaneen, D. Rohe and H. Müther, Phys. Rev. C 70: 024309, (2004).

[4]   Kh.S.A. Hassaneen and H. Müther, Phys. Rev. C 70: 054308, (2004).

[5]   V.G.J. Stoks, R.A.M. Klomp, C.P.F. Terheggen and J.J.D. Swart, Construction of high-quality NN potential models. Phys. Rev. C 49: 2950-2962. DOI: 10.1103/PhysRevC.49. 2950, (1994)

[6]   R.B. Wiringa, V.G.J. Stoks and R. Schiavilla, Phys. Rev. C 51: 38, (1995).

[7]   R. Machleidt, F. Sammarruca and Y. Song, Phys. Rev. C 53: R1483, (1996); R. Machleidt, Phys. Rev., C 63: 024001, (2001).

[8]   T. Frick and H. Müther, Phys. Rev. C 68: 034310, (2003).

[9]   A.E.L. Dieperink, Y. Dewulf, D.V. Neck, M. Waroquier and V. Rodin, Phys. Rev. C 68: 064307, (2003).

[10] W. Zuo, I. Bombaci and U. Lombardo, Asymmetric nuclear matter from an extended Brueckner-Hartree-Fock approach. Phys. Rev. C 60: 024605-024617. DOI: 10.1103/PhysRevC. 60.024605, (1999).

[11] I. Vidana and I. Bombaci, Equation of state and magnetic susceptibility of spin polarized isospin asymmetric nuclear matter. Phys. Rev. C 66: 045801-045811. DOI:10.1103/Phys RevC.66.045801, (2002).

[12] K.A. Brueckner and J.L. Gammel, Properties of nuclear matter. Phys. Rev. 109: 1023-1039. DOI: 10.1103/PhysRev. 109.1023, (1958).

[13] H. Müther, M. Prakash and T.L. Ainsworth, The nuclear symmetry energy in relativistic Brueckner-Hartree-Fock calculations. Phys. Lett. B 199: 469-474. DOI: 10.1016/0370 -2693(87)91611-X , (1987).

[14] L. Engivik, M. Hjorth-Jensen, E. Osnes, G. Bao and E. Ostgaard, Asymmetric nuclear matter and neutron star properties. Phys. Rev. Lett. 73: 2650-2653. DOI: 10.1103/ PhysRevLett.73.2650, (1994).

[15] F. Hofmann, C.M. Keil and H. Lenske, Density dependent hadron field theory for asymmetric nuclear matter and exotic nuclei. Phys. Rev. C 64: 034314-034229. DOI: 10.1103/Phys RevC.64.034314, (2001).

[16] D. Alonso and F. Sammarruca, Microscopic calculations in asymmetric nuclear matter. Phys. Rev. C 67: 054301-054301. DOI: 10.1103/PhysRevC.67.054301, (2003).

[17] I. Bombaci and U. Lombardo, Asymmetric nuclear matter equation of state. Phys. Rev. C 44: 1892-1900. DOI: 10.1103/PhysRevC.44.1892, (1991).

[18] H.Q. Song, M. Baldo, G. Giansiracusa, U. Lombardo, Phys. Rev. Lett. 81, 1584, (1998).

[19] R.B. Wiringa, V. Fiks and A. Fabrocini, Phys. Rev. C 38: 1010, (1988).

[20] A. Akmal and V.R. Pandharipande, Phys. Rev. C 56: 2261, (1997).

[21] Y. Sugahara and H. Toki, Nucl. Phys. A 579: 557, 1994; Akmal, A., V.R. Pandharipande and D.G. Ravenhall, Phys. Rev. C 58: 1804, (1998).

[22] D. Vretenar, T. Niksic and P. Ring, Phys. Rev. C 68: 024310. (2003).

[23] J.R. Stone, P.D. Stevenson, J.C. Miller and M.R. Strayer, Phys. Rev. C 65: 064312, (2002).

[24] J.R. Stone, J.C. Miller, R. Koncewicz, P.D. Stevenson and M.R. Strayer, Phys. Rev. C 68: 034324, (2003).

[25] P. Bozek, Phys. Lett. B 586: 239, (2004).

[26] N.M. Hugenholtz and L.V. Hove, Physica 24: 363, (1958).

[27] K. Gad, Eur. Phys. J. A 22: 405, (2004).

[28] P. Bozek and P. Czerski, Eur. Phys. J. A 11: 271, (2001).

[29] P. Bozek, Eur. Phys. J. A 15: 325, (2002).

[30] W. Zuo, G. Giansiracusa, U. Lombardo, N. Sandulescu and H.J. Schulze, Single-particle properties in neutron matter from extended Brueckner theory. Phys. Lett. B 421: 1-7. DOI: 10.1016/S0370-2693(97)01600-6, (1998).

[31] B.A. Li, L.W. Chen and C.M. Ko, Recent progress and new challenges in isospin physics with heavy-ion reactions. Phys. Rep. 464: 113-281. DOI: 10.1016/j.physrep.2008.04.005, (2008).

[32] V. Baran, M. Colonna, V. Greco and M.D. Toro, Reaction dynamics with exotic nuclei. Phys. Rep. 410: 335-466. DOI:

10.1016/j.physrep.2004.12.004, (2005).

[33] K. Gad and Kh.S.A. Hassaneen, Equation of state for neutron-rich matter with self-consistent green function approach. Nucl. Phys. A 793: 67-78. DOI: 10.1016/j.nuclphysa.2007.06.015, (2007).

[34] Kh. Hassaneen and K. Gad, The nuclear symmetry energy in self-consistent green-function calculations. J. Phys. Soc. Jpn. 77: 084201-084206. DOI: 10.1143/JPSJ.77.084201, (2008).

[35] P. Gögelein, E.N.E.V. Dalen, K. Gad, Kh.S.A. Hassaneen and H. Müther, Properties of asymmetric nuclear matter in different approaches. Phys. Rev. C 79: 024308-024320. DOI: 10.1103/PhysRevC.79.024308, (2009).

[36] Z.H. Li, U. Lombardo, H.J. Schulze, L.W. Zuo and L.W. Chen, Nuclear matter saturation point and symmetry energy with modern nucleon-nucleon potentials. Phys. Rev. C 74: 047304-047307. DOI: 10.1103/PhysRevC.74.047304, (2006).

[37] M.I. Haftel and F. Tabakin, Nuclear saturation and the smoothness of nucleon-nucleon potentials. Nucl. Phys. A 158: 1-42. DOI: 10.1016/0375-9474(70)90047-3, (1970).

[38] C. Mahaux and R. Sartor, Adv. Nucl. Phys. 20: 1, (1991).

[39] P. Grange, J. Cugnon and A. Lejeune, Nucl. Phys. A 473: 365, (1987).

[40] A. L. Fetter and J. D. Walecka, *Quantum Theory of Many Particle Physics* (McGraw-Hill, New York), (1971).

[41] P. A. Henning, Phys. Rept. 253: 235, (1995).

[42] C. Bloch, Nucl. Phys. 7: 451 (1958); C. Bloch and C. De Domicis, Nucl. Phys. 7, 459; 10: 509, (1958).

[43] M. Baldo and L.S. Ferreira, Nuclear liquid-gas phase transition. Phys. Rev. C 59: 682-703. DOI: 10.1103/PhysRevC.59.682, (1999).

[44] H. Mansour, M. Hammad, and M.Y.M. Hassan, Phys. Rev. C 56: 1418, (1997).

[45] M. Barranco and J. Treiner, Self-consistent description of nuclear of level densities. Nucl. Phys. A 351: 269-284. DOI: 10.1016/0375-9474(81)90444-9, (1981).

[46] Kh.S.A. Hassaneen, H.M. Abo-Elsebaa, E.A. Sultan and H. Mansour, Nuclear binding energy and symmetry energy of nuclear matter with modern nucleon-nucleon potentials. Annals Phys. 326: 566-577. DOI: 10.1016/j.aop.2010.11.010, (2011)

[47] M. Baldo and A. Fiasconaro, Single particle spectrum and binding energy of nuclear matter. Phys. Lett. B 491: 240-244. DOI: 10.1016/S0370-2693(00)01052-2, (2000)

[48] B.D. Day, Nuclear Saturation from Two-Nucleon Potentials. Phys. Rev. Lett. 47: 226-229. DOI:10.1103/PhysRevLett.47.226, (1981).

[49] M. Hjorth-Jensen, T.T.S. Kuo, and E. Osnes, Phys. Rep. 261: 125, (1995).

[50] V. Somua and P. Bozek, Phys. Rev. C 78: 054003, (2008).

[51] M. Baldo and A.E. Shaban, Phys. Lett. B 661: 373, (2008).

[52] I. Bombaci and U. Lombardo, Phys. Rev. C 44: 1892, (1991).

[53] P.E. Haustein, An overview of the 1986-1987 atomic mass predictions. Atomic Data Nuclear Data Tables, 39: 185-200. DOI: 10.1016/0092-640X(88)90019-8, (1988).

[54] B.A. Li, Nucl. Phys. A 708: 365, (2002).

[55] I. Vidana, A. Polls, A. Ramos, L. Engvik and M. Mjorth-Jensen, Phys. Rev. C 62: 035801, (2000).

[56] M. Baldo, G.F. Burgio and H.J. Schulze, Phys. Rev. C 61: 055801, (2000).

[57] P. Gögelein, E.N.E.V. Dalen, C. Fuchs and H. Müther, Phys. Rev. C 77: 025802, (2008).

[58] A.E.L. Dieperink, Y. Dewulf, D.V. Neck, M. Waroquier and V. Rodin, Phys. Rev. C 68: 064307, (2003).

[59] P. Gögelein and H. Müther, Phys. Rev. C 76: 024312, (2007).

[60] L. Engvik, G. Bao, M. Hjorth-Jensen, E. Osnes, and E. Oestaard, Astrophys. J. 469: 794, (1996).

[61] J.R. Stone and P.G. Reinhard, Prog. Part. Nucl. Phys. 56: 587, (2007).

[62] P. Ring and P. Schuck, The Nuclear Many Body Problem, (Springer, Berlin Heidelberg New York, 1980).

[63] M. Bender, P.H. Heenen, and P.G. Reinhard, Rev. Mod. Phys. 75: 121, (2003).

[64] W. Zuo, L.G. Cao, B.A. Li, U. Lombardo and C.W. Shen, Phys. Rev. C 72: 014005, (2005).

[65] A.M. Lane, Nucl. Phys. 35: 676, (1962).

[66] I. Bombaci, A. Polls, A. Ramos, A. Rios, and I. Vidaña, Phys. Lett. B 632: 638, (2006).

[67] A. Rios, A. Polls, and I. Vidaňa, Phys. Rev. C 71: 055802, (2005).

[68] H. Mansour and Kh.S.A. Hassaneen, Nuclear and neutron matter properties using BHF approximation, Jour. Nucl. Part. Phys. 2(2): 14-21, DOI: 10.5923/j.jnpp.2012202.04, (2012).

[69] H. Mansour, K. Gad, and Kh.S.A. Hassaneen, Self-Consistent Green Function Calculations for Isospin Asymmetric Nuclear Matter, Prog. Theor. Phys. 123: 687-700. DOI: 10.1143/PTP.123.687 , (2010).